

Journal Pre-proof

Single-cell RNA seq-derived signatures define response patterns to atezolizumab + bevacizumab in advanced hepatocellular carcinoma



Sarah Cappuyns, Marta Piqué-Gili, Roger Esteban-Fabré, Gino Philips, Ugne Balaseviciute, Roser Pinyol, Albert Gris-Oliver, Vincent Vandecaveye, Jordi Abril-Fornaguera, Carla Montironi, Laia Bassaganyas, Judit Peix, Marcus Zeitlhoefler, Agavni Mesropian, Júlia Huguet-Pradell, Philipp K. Haber, Igor Figueiredo, Giorgio Ioannou, Edgar Gonzalez-Kozlova, Antonio D'Alessio, Raphael Mohr, Tim Meyer, Anja Lachenmayer, Jens U. Marquardt, Helen L. Reeves, Julien Edeline, Fabian Finkelmeier, Jörg Trojan, Peter R. Galle, Friedrich Foerster, Beatriz Minguez, Robert Montal, Sacha Gnjatic, David J. Pinato, Mathias Heikenwalder, Chris Verslype, Eric Van Cutsem, Diether Lambrechts, Augusto Villanueva, Jeroen Dekervel, Josep M. Llovet

PII: S0168-8278(24)02771-5

DOI: <https://doi.org/10.1016/j.jhep.2024.12.016>

Reference: JHEPAT 9927

To appear in: *Journal of Hepatology*

Received Date: 2 February 2024

Revised Date: 29 November 2024

Accepted Date: 7 December 2024

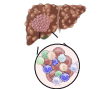
Please cite this article as: Cappuyns S, Piqué-Gili M, Esteban-Fabré R, Philips G, Balaseviciute U, Pinyol R, Gris-Oliver A, Vandecaveye V, Abril-Fornaguera J, Montironi C, Bassaganyas L, Peix J, Zeitlhoefler M, Mesropian A, Huguet-Pradell J, Haber PK, Figueiredo I, Ioannou G, Gonzalez-Kozlova E, D'Alessio A, Mohr R, Meyer T, Lachenmayer A, Marquardt JU, Reeves HL, Edeline J, Finkelmeier F, Trojan J, Galle PR, Foerster F, Minguez B, Montal R, Gnajatic S, Pinato DJ, Heikenwalder M, Verslype C, Van Cutsem E, Lambrechts D, Villanueva A, Dekervel J, Llovet JM, Single-cell RNA seq-derived signatures define response patterns to atezolizumab + bevacizumab in advanced hepatocellular carcinoma, *Journal of Hepatology*, <https://doi.org/10.1016/j.jhep.2024.12.016>.

This is a PDF file of an article that has undergone enhancements after acceptance, such as the addition of a cover page and metadata, and formatting for readability, but it is not yet the definitive version of

record. This version will undergo additional copyediting, typesetting and review before it is published in its final form, but we are providing this version to give early visibility of the article. Please note that, during the production process, errors may be discovered which could affect the content, and all legal disclaimers that apply to the journal pertain.

© 2024 The Author(s). Published by Elsevier B.V. on behalf of European Association for the Study of the Liver.

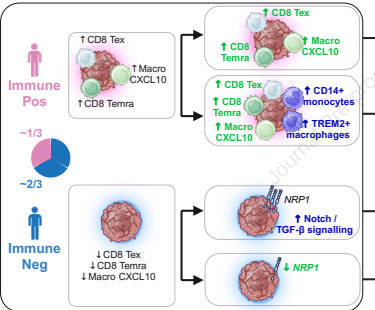
Advanced hepatocellular carcinoma



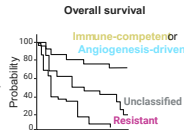
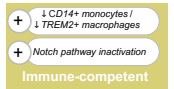
scRNAseq

Atezolizumab + bevacizumab

Determinants of response and primary resistance to atezolizumab + bevacizumab



Molecular subsets of clinical outcome to atezolizumab + bevacizumab



1 **Title:** Single-cell RNA seq-derived signatures define response patterns to
2 **atezolizumab + bevacizumab in advanced hepatocellular carcinoma**

3

4 **Short Title:** Two distinct responses to atezo+bev in advanced HCC

5

6 **Authors and affiliations**

7 Sarah Cappuyns^{1,2,3,4,5}, Marta Piqué-Gili^{5,6}, Roger Esteban-Fabró^{5,6}, Gino Philips^{3,4},
8 Ugne Balaseviciute⁶, Roser Pinyol⁶, Albert Gris-Oliver⁶, Vincent Vandecaveye^{7,8}, Jordi
9 Abril-Fornaguera^{5,6}, Carla Montironi^{6,9}, Laia Bassaganyas¹⁰, Judit Peix⁶, Marcus
10 Zeitlhoefler⁵, Agavni Mesropian^{5,6}, Júlia Huguet-Pradell^{5,6}, Philipp K. Haber¹¹, Igor
11 Figueiredo¹², Giorgio Ioannou¹², Edgar Gonzalez-Kozlova¹², Antonio D'Alessio¹³,
12 Raphael Mohr¹⁴, Tim Meyer¹⁵, Anja Lachenmayer¹⁶, Jens U. Marquardt¹⁷, Helen L.
13 Reeves¹⁸, Julien Edeline¹⁹, Fabian Finkelmeier²⁰, Jörg Trojan²⁰, Peter R. Galle²¹,
14 Friedrich Foerster²¹, Beatriz Mínguez²², Robert Montal²³, Sacha Gnjatic¹², David J.
15 Pinato^{13,24}, Mathias Heikenwalder²⁵, Chris Verslype^{1,2}, Eric Van Cutsem^{1,2}, Diether
16 Lambrechts^{3,4}, Augusto Villanueva⁵, Jeroen Dekervel^{1,2*}, Josep M. Llovet^{5,6,26*}

17

18

19 ¹Digestive Oncology, Department of Gastroenterology, University Hospitals Leuven,
20 Leuven, Belgium.

21 ²Laboratory of Clinical Digestive Oncology, Department of Oncology, KU Leuven,
22 Leuven, Belgium.

23 ³Laboratory for Translational Genetics, Department of Human Genetics, KU Leuven,
24 Leuven, Belgium.

25 ⁴VIB Centre for Cancer Biology, Leuven, Belgium.

26 ⁵Mount Sinai Liver Cancer Program (Divisions of Liver Diseases, Department of
27 Hematology/Oncology, Department of Medicine), Tisch Cancer Institute, Icahn School
28 of Medicine at Mount Sinai, New York, USA.

29 ⁶Liver Cancer Translational Research Laboratory, Institut d'Investigacions
30 Biomèdiques August Pi i Sunyer (IDIBAPS), Hospital Clínic, Universitat de Barcelona,
31 Barcelona, Catalonia, Spain.

32 ⁷Radiology Department, University Hospitals Leuven, Leuven, Belgium.

33 ⁸Laboratory of Translational MRI, Department of Imaging and Pathology, KU Leuven,
34 Leuven, Belgium.

35 ⁹Pathology Department and Molecular Biology Core, Hospital Clínic of Barcelona,
36 Barcelona, Spain.

37 ¹⁰Institut de Génomique Fonctionnelle, Univ. Montpellier, CNRS, INSERM,
38 Montpellier, France.

39 ¹¹Department of Surgery, Campus Charité Mitte and Campus Virchow-Klinikum,
40 Charité-Universitätsmedizin Berlin, 13353 Berlin, Germany.

41 ¹²Department of Immunology and Immunotherapy, Icahn School of Medicine at Mount
42 Sinai, New York, NY, USA.

43 ¹³Department of Surgery & Cancer, Imperial College London, Hammersmith Hospital,
44 London, United Kingdom.

45 ¹⁴Department of Hepatology and Gastroenterology, Charité - Universitätsmedizin
46 Berlin, Campus Virchow Klinikum (CVK) and Campus Charité Mitte (CCM), Berlin,
47 Germany.

48 ¹⁵Research Department of Oncology, UCL Cancer Institute, University College
49 London, Royal Free Hospital, London, UK.

- 50 ¹⁶Department of Visceral Surgery and Medicine, Inselspital, Bern University Hospital,
51 University of Bern, Bern, Switzerland.
- 52 ¹⁷Department of Medicine I, University Medical Center Schleswig Holstein Campus
53 Lübeck, Lübeck, Germany.
- 54 ¹⁸Newcastle University Translational and Clinical Research Institute and Newcastle
55 University Centre for Cancer, Medical School, Framlington Place, Newcastle Upon
56 Tyne, NE2 4HH, UK; Hepatopancreatobiliary Multidisciplinary Team, Newcastle upon
57 Tyne NHS Foundation Trust, Freeman Hospital, Newcastle upon Tyne, UK.
- 58 ¹⁹Department of Medical Oncology, Centre Eugène Marquis, Rennes, France.
- 59 ²⁰Department of Gastroenterology, University Liver and Cancer Centre, Frankfurt,
60 Germany.
- 61 ²¹Department of Medicine I, University Medical Center of the Johannes-Gutenberg
62 University, Mainz, Germany.
- 63 ²²Liver Unit, Hospital Universitari Vall d'Hebron, Vall d'Hebron Barcelona Hospital
64 Campus, Barcelona, Spain, Liver Diseases Research Group, Vall d'Hebron Institute
65 of Research (VHIR), Vall d'Hebron Barcelona Hospital Campus, Barcelona, Spain,
66 CIBERehd, Universitat Autònoma de Barcelona, Barcelona, Spain.
- 67 ²³Department of Medical Oncology, Cancer Biomarkers Research Group, Hospital
68 Universitari Arnau de Vilanova, IRBLleida, University of Lleida (UdL), Catalonia, Spain.
- 69 ²⁴Department of Surgery & Cancer, Imperial College London, Hammersmith Hospital,
70 London, United Kingdom.
- 71 ²⁵Division of Chronic Inflammation and Cancer, German Cancer Research Center
72 (DKFZ), Heidelberg, Germany.
- 73 ²⁶Institució Catalana de Recerca i Estudis Avançats (ICREA), Barcelona, Catalonia,
74 08010, Spain.

75

76 **Shared first authorship**

77 *Equal contributions

78

79 **Word count:** 6866

80 **Number of figures:** 7

81

82 **Correspondence**

83 * Josep M. Llovet, M.D., Ph.D., Mount Sinai Liver Cancer Program, Division of Liver
84 Diseases, Tisch Cancer Institute, Icahn School of Medicine at Mount Sinai, New York,
85 NY, USA. E-mail: josep.llovet@mountsinai.org

86 * Jeroen Dekervel, M.D, Ph.D., Digestive Oncology, Department of Gastroenterology
87 and Hepatology, UZ/KU Leuven, Belgium. E-mail: jeroen.dekervel@uzleuven.be

88

89 **Keywords:** Advanced Hepatocellular Carcinoma; Atezolizumab and bevacizumab;
90 Biomarkers of Response; Single-Cell RNA-Sequencing; Primary Resistance

91

92 **Funding**

93 SC was supported by a strategic basic research fellowship from Research
94 Foundation— Flanders (FWO; 1S95221N) and a post-doctoral fellowship from the
95 Belgian American Educational Foundation (BAEF). MPG was supported by a pre-
96 doctoral grant from the Spanish National Health Institute (MICINN, PRE2020-094716)
97 and a mobility grant from “Fundació Universitària Agustí Pedro i Pons”. REF was
98 supported by a predoctoral grant from the Spanish National Health Institute (MCINN;
99 BES-2017-081286) and a mobility grant from “Fundació Universitària Agustí Pedro i

100 Pons". UB was supported by the EILF-EASL Juan Rodés PhD Studentship from the
101 European Association for the Study of the Liver (EASL) and the EASL International
102 Liver Foundation (EILF). RP is supported by the Fundació de Recerca Clínic
103 Barcelona - IDIBAPS and by a grant from the Spanish National Health Institute
104 (MICINN, PID2022-139365OB-I00, funded by MICIU/AEI/10.13039/501100011033
105 and FEDER). JAF was supported by a doctoral training grant from the University of
106 Barcelona (PREDOCS-UB 2020) and by the "Societat Catalana de Digestologia"
107 mobility grant. JP was supported by a PERIS ICT-Suport grant from the "Departament
108 de Salut de la Generalitat de Catalunya" (SLT017/20/000206). AM was supported by
109 the Generalitat of Catalonia with a FI-SDUR fellowship (2021 FISDU 00338) from
110 AGAUR. JHP was supported by the predoctoral grant "Ayudas para la Formación de
111 Profesorado Universitario (FPU)" (FPU21/03361) and a mobility grant from "Fundació
112 Universitària Agustí Pedro i Pons". MZ was funded by the Deutsche
113 Forschungsgemeinschaft (DFG, German Research Foundation; 531006414). AD is
114 supported by the National Institute for Health Research (NIHR) Imperial BRC, by grant
115 funding from the European Association for the Study of the Liver (2021 Andrew
116 Burroughs Fellowship) and from Cancer Research UK (RCCPDB- Nov21/100008).
117 HLR is supported by Cancer Research UK (CRUK) programme grant C18342/A23390,
118 Accelerator award C9380/A26813, the CRUK Newcastle Centre CTRQQR-
119 2021\100003; the NIHR Newcastle Biomedical Research Centre awarded to the
120 Newcastle upon Tyne Hospitals NHS Foundation Trust and Newcastle University
121 (grant ref: 570556) and the European Commission (Horizon Europe-Mission Cancer,
122 THRIVE, Ref. 101136622). RM acknowledges the support from ISCIII (PI21/01619
123 research project and Juan Rodés contract), SEOM (research project), TTD (research
124 project) and Fundación MERCK Salud (research project). SG was partially supported

125 by NIH grants CA224319, DK124165, CA234212, and CA196521. DJP is supported
126 by grant funding from the Wellcome Trust Strategic Fund (PS3416), the Associazione
127 Italiana per la Ricerca sul Cancro (AIRC MFAG 25697) and acknowledges grant
128 support from the Cancer Treatment and Research Trust (CTRT), the Foundation for
129 Liver Research and infrastructural support by the Imperial Experimental Cancer
130 Medicine Centre and the NIHR Imperial Biomedical Research Centre. The views
131 expressed are those of the authors and not necessarily those of the NHS, the NIHR,
132 or the Department of Health and Social Care. DL was supported by an ERC Advanced
133 Grant (101055422) and a KU Leuven Internal Fund (C14/18/092). JML is supported
134 by grants from European Commission (Horizon Europe-Mission Cancer, THRIVE, Ref.
135 101136622), the NIH (R01-CA273932-01, R01DK56621 and R01DK128289); Samuel
136 Waxman Cancer Research Foundation; the Spanish National Health Institute
137 (MICINN, PID2022-139365OB-I00, funded by MICIU/AEI/10.13039/501100011033
138 and FEDER); Cancer Research UK (CRUK), Fondazione AIRC per la Ricerca sul
139 Cancro and Fundación Científica de la Asociación Española Contra el Cáncer
140 (FAECC) (Accelerator Award, HUNTER, Ref. C9380/A26813); the “la Caixa” Banking
141 Foundation; Acadèmia de Ciències Mèdiques i de la Salut de Catalunya i Balears;
142 Fundación Científica de la Asociación Española Contra el Cáncer (FAECC; Proyectos
143 Generales, Ref. PRYGN223117LLOV; and Reto AECC 70% Supervivencia: Ref.
144 RETOS245779LLOV) and the Generalitat de Catalunya/AGAUR (2021 SGR 01347).

145

146 **Disclosures**

147 AD received educational support for congress attendance and consultancy fees from
148 Roche, and speaker fees from Roche, AstraZeneca, Eisai, and Chugai. FFo has
149 received honoraria for lectures from AstraZeneca, Lilly, MSD, Pfizer and Roche. He

150 has served as advisory board member to AstraZeneca, BMS, Eisai and Roche and
151 has received travel support from Merck KGaA and Servier. RM has received
152 consulting and lecture fees from Servier, Roche and Bristol Myers Squibb and travel
153 and education funding from MSD, Eli Lilly, Bayer, Roche, AstraZeneca. SG reports
154 other research funding from Boehringer Ingelheim, Bristol-Myers Squibb, Celgene,
155 Genentech, Regeneron, and Takeda not related to this study. SG is a named co-
156 inventor on an issued patent for MICSSS, a multiplex immunohistochemistry to
157 characterize tumours and treatment responses. The technology is filed through Icahn
158 School of Medicine at Mount Sinai (ISMMS) and is currently unlicensed. AV has
159 received consulting fees from FirstWorld, Natera, Pioneering Medicine and
160 Genentech; advisory board fees from BMS, Roche, Astra Zeneca, Eisai, and NGM
161 Pharmaceuticals; and research support from Eisai. He has stock options from
162 Espervita. JML is receiving research support from Eisai Inc, Bristol-Myers Squibb
163 Bayer HealthCare Pharmaceuticals, and Ipsen, and consulting fees from Eisai Inc,
164 Merck, Bristol-Myers Squibb, Eli Lilly, Roche, Genentech, Ipsen, Glycotest,
165 AstraZeneca, Omega Therapeutics, Bayer HealthCare Pharmaceuticals, Mina Alpha,
166 Boston Scientific, Exelixis, Bluejay and Captor Therapeutics. The remaining authors
167 have no conflicts of interest to declare.

168

169 **Author's contributions**

170 JD and JML designed and jointly supervised the study, with help from DL and AV.
171 Clinical samples were established and clinically annotated by SC, MPG, MZ, VV, PKH,
172 AD, RMoh, TM, AL, JUM, HLR, JE, FF, JT, PG, FFFo, BM, RM, DJP, CV, EVC, JD and
173 JML. Data analysis was performed by SC, MPG and REF with substantial help from
174 GP. REF designed the integrative model and created PredictOR with contributions

175 from SC and MPG. CM contributed to the pathological characterisation of tumour
176 samples. LB contributed to the analysis of genomic data. UB, JP, AM, and JHP were
177 involved in sample processing including RNA isolation. IF, GI, EGK and SG
178 contributed to the multiplexed immunohistochemical (IHC) consecutive staining on
179 single slide (MICSSS) analysis. RP, AGO, JAF, MH, CV and EVC provided scientific
180 input and contributed to critical data interpretation. The manuscript was written by SC
181 and MPG with substantial contribution from REF and under supervision of JD and JML.
182 All authors read or provided comments on the manuscript.

183

184 **Data availability statement**

185 RNA sequencing data of the Inhouse RNAseq Cohort, generated for the purpose of
186 this study, will be deposited at the European Genome phenome Archive (EGA;
187 <https://ega-archive.org>) upon publication.

188 **Abstract**

189 **Background & Aims**

190 The combination of atezolizumab and bevacizumab (atezo+bev) is the current
191 standard of care for advanced hepatocellular carcinoma (HCC), providing a median
192 overall survival (OS) of 19.2 months. Here, we aim to uncover the underlying cellular
193 processes driving clinical benefit versus resistance to atezo+bev.

194 **Methods**

195 We harnessed the power of single-cell RNA sequencing in advanced HCC to derive
196 gene expression signatures recapitulating 21 cell phenotypes. These signatures were
197 applied to 422 RNA-sequencing samples of advanced HCC patients treated with
198 atezo+bev (n=317) versus atezolizumab (n=47) or sorafenib (n=58) as comparators.

199 **Results**

200 We unveiled two distinct patterns of response to atezo+bev. First, an immune-
201 mediated response characterized by the combined presence of CD8+ T effector cells
202 and pro-inflammatory CXCL10+ macrophages, representing an immune rich
203 microenvironment. Second, a non-immune, angiogenesis-related response
204 distinguishable by a reduced expression of the VEGF co-receptor neuropilin-1 (*NRP1*),
205 a biomarker that specifically predicts improved OS upon atezo+bev vs sorafenib (p =
206 0.039). Primary resistance was associated with an enrichment of immunosuppressive
207 myeloid populations, namely CD14+ monocytes and TREM2+ macrophages, and
208 Notch pathway activation. Based on these mechanistic insights we define "*Immune-*
209 *competent*" and "*Angiogenesis-driven*" molecular subgroups, each associated with a
210 significantly longer OS with atezo+bev versus sorafenib (p of interaction = 0.027), and
211 a "*Resistant*" subset.

212 **Conclusion**

213 Our study unveils two distinct molecular subsets of clinical benefit to atezolizumab plus
214 bevacizumab in advanced HCC (“*Immune-competent*” and “*Angiogenesis-driven*”) as
215 well as the main traits of primary resistance to this therapy, thus providing a molecular
216 framework to stratify patients based on clinical outcome and guiding potential
217 strategies to overcome resistance.

218

219

220 **Impact and implications**

221 Atezolizumab + bevacizumab (atezo+bev) is the standard-of-care treatment in
222 advanced hepatocellular carcinoma (HCC), yet molecular determinants of clinical
223 benefit to the combination remain unclear. This study harnesses the power of single-
224 cell RNA sequencing, deriving gene expression signatures representing 21 cell
225 subtypes in the advanced HCC microenvironment. By applying these signatures to
226 RNA-sequencing samples, we reveal two distinct response patterns to atezo+bev and
227 define molecular subgroups of patients (“*Immune-competent*” and “*Angiogenesis-
driven*” versus “*Resistant*”) with differential clinical outcomes upon treatment with
228 atezo+bev, pointing towards the role of immunosuppressive myeloid cell types and
229 Notch pathway activation in primary resistance to atezo+bev. These results may help
230 refine treatment strategies and improve outcomes for patients with advanced HCC,
231 while also guiding future research aimed at overcoming resistance mechanisms.

233 **Introduction**

234 Hepatocellular carcinoma (HCC) is the third leading cause of cancer-related mortality
235 worldwide¹, and incidence rates are rising rapidly. Approximately 50-60% of HCC
236 patients eventually evolve to advanced stages of the disease requiring systemic
237 therapies². In 2020, the combination of atezolizumab, an anti-PDL1 immune
238 checkpoint inhibitor (ICI), and bevacizumab, a VEGFA inhibitor (hereafter, atezo+bev),
239 demonstrated significantly improved survival compared to sorafenib, the standard of
240 care for over a decade³, in the IMbrave150 phase III randomized study (19.2 vs 13.4
241 months)^{4,5}. Thus, atezo+bev was established as the new standard of care in advanced
242 HCC, achieving an objective response in ~35% of patients. However, the molecular
243 determinants of clinical benefit from the combination are yet to be robustly defined⁶⁻⁸.
244 The tumour-microenvironment (TME) plays a crucial role in HCC development and
245 progression, mediating response and/or resistance to immunotherapy^{7,9}. Several gene
246 expression signatures that recapitulate inflamed classes of HCC or inflammatory
247 signalling have been associated with response to single-agent anti-PD1¹⁰⁻¹⁴.
248 Consistently, pre-existing tumour immunity – namely high PD-L1 expression, a T-
249 effector signature¹⁵ and high intra-tumoural CD8+ T cell density – was associated with
250 better clinical outcomes in atezo+bev-treated patients, and an “atezo+bev response
251 signature” (ABRS) was derived⁶. However, a general issue when generating genomic
252 signatures is the lack of biological insights or mechanistic rationale that links selected
253 genes with outcome. Consequently, so far, none of these gene signatures have made
254 it to clinically validated biomarkers of response to systemic therapy in advanced HCC⁸.
255 Recent advances in single-cell RNA sequencing (scRNAseq) have become key to
256 study phenotypical and functional diversity of tumour-infiltrating stromal and immune
257 cells, allowing the exploration of the TME of advanced HCC and how it relates to ICI-

258 response^{16–18}. However, single-cell sequencing technologies are not suitable for use
259 in routine clinical practice.

260 Here, using scRNAseq data of 31 advanced HCC tumours, we generate cell-type
261 specific gene signatures representing 21 distinct cell phenotypes. We then explore
262 their potential as predictive biomarkers of atezo+bev response using bulk
263 transcriptomic data from 422 pre-treatment advanced HCC samples. We unveil two
264 distinct subtypes of responders to atezo+bev: a first subgroup is defined by the
265 combined intra-tumoural presence of two CD8+ effector T cell subtypes and CXCL10+
266 macrophages, representing an immune-rich TME, while a second subgroup of
267 responders lacks infiltration by these three immune-related cell types and is
268 distinguished by a reduced expression of the VEGF co-receptor neuropilin-1 (*NRP1*).
269 Moreover, we highlight the role of immunosuppressive cells and Notch activation in
270 primary resistance to atezo+bev. Finally, patients were categorized accordingly into
271 molecular subsets predictive of clinical benefit or resistance to atezo+bev.

272

273

274 **Materials and Methods**275 Study design

276 We aimed to leverage the single cell resolution offered by scRNAseq technologies to
277 generate gene signatures that can be applied to RNAseq data analysis (**Fig. 1**). We
278 first used scRNAseq data to generate gene signatures representative of the cellular
279 heterogeneity present in the TME of advanced HCC¹⁷. These gene signatures were
280 then applied to RNAseq cohorts to identify response subtypes and determinants of
281 response versus resistance to atezo+bev.

282

283 Patient cohorts and sample collection

284 This study encompasses six cohorts. An overview is provided in **Table S1** (see
285 **Supplementary Methods** for details).

286

287 The **scRNAseq Discovery Cohort**¹⁷ and **scRNAseq Validation Cohort**¹⁸ include a
288 total of 47 advanced HCC tumours, taken prior to start of systemic treatment. Samples
289 were subjected to scRNAseq and used to generate and validate scRNAseq-derived
290 gene signatures.

291

292 The **Inhouse RNAseq Cohort** and **External RNAseq Cohort**⁶ comprise a total of 422
293 pre-treatment HCC tumour samples subjected to RNAseq. Patients were treated with
294 atezo+bev (n=317), atezolizumab (n=47) or sorafenib (n=58) and stratified into
295 responders versus non-responders according to best objective response¹⁹.
296 Responders displayed either Complete (CR) or Partial Response (PR), while non-
297 responders were defined as those patients with Stable Disease (SD) or Progressive
298 Disease (PD). Disease control comprises CR, PR and SD as best response.

299 Secondary endpoints were overall survival (OS) and progression free survival (PFS).

300 See **Fig. S1** for details.

301

302 The **External WES Cohort**⁶ and the **Anti-PD1 Validation Cohort**¹⁰ are described in

303 **Supplementary Methods**.

304

305 Generating scRNAseq-derived gene signatures

306 Using a tailored bio-informatics pipeline, adapted from a previous study²⁰, we

307 generated scRNAseq-derived gene signatures for the 35 cell (pheno-)types identified

308 at the single-cell resolution in the scRNAseq Discovery Cohort¹⁷. Starting from the fully

309 annotated single-cell dataset, we performed differential gene expression (DGE)

310 analysis to identify differentially expressed genes (DEG) for each cell (pheno-)type

311 using the *FindAllMarkers* function from Seurat 4²¹. DEGs were selected based on the

312 Wilcoxon rank sum test, restricted to genes expressed in at least 10% of cells.

313 Ribosomal, mitochondrial and immunoglobulin genes were removed and only genes

314 with average log2-fold change ≥ 1.5 were selected, hypothesizing that DEGs above

315 this threshold would be captured in RNAseq data.

316 To generate cell type-specific gene signatures, we further filtered the resulting list of

317 up- versus down-regulated DEGs, separately. An overview is provided in **Fig. S2A**.

318 Please refer to **Supplementary Methods** for details on DEG filtering steps and

319 signature categorization as specific or not specific.

320 In sum, we generated ‘specific’ gene signatures to identify 21 distinct cell (pheno-

321)types present in the TME of advanced HCC (**Fig. 2B; Fig. S3**). An overview of the

322 scRNAseq-derived gene signatures is provided in **Table S2**.

323

324 For details on the characterization and validation of the scRNAseq-derived gene
325 signatures, as well as the analysis and statistics of bulk transcriptomics, genomic WES
326 data, experimental models of HCC, flow cytometry and multiplexed
327 immunohistochemistry data, please refer to **Supplementary Methods**.

328

329 Definition of molecular subsets of atezo+bev clinical outcome

330 Patients from the External RNAseq Cohort treated with atezo+bev were categorized
331 according to the presence or absence of the scRNAseq-derived gene signatures
332 recapitulating CD8 Temra, CD8 Tex, Macro CXCL10, TREM2+ macrophage and
333 CD14+ monocyte immune populations, as well as into having Notch pathway
334 activation versus inactivation based on a previously reported signature in HCC²².
335 Additionally, patients were classified as NRP1-Low if tumour NRP1 expression was ≤
336 0.75 of the mean in adjacent liver tissue, and as NRP1-High otherwise. For details on
337 the classification criteria into “*Immune-competent*”, “*Angiogenesis-driven*” and
338 “*Resistant*” molecular subsets, please refer to **Supplementary Methods**.

339

340 **Results**341 Generation of specific, robust and biologically plausible gene signatures capturing cell
342 phenotypes identified from scRNAseq in advanced HCC

343 Here, we aimed to leverage the single cell resolution offered by scRNAseq
344 technologies to generate gene signatures that are applicable to conventional RNAseq
345 data analysis, a more widely available technique. Thus, these gene signatures could
346 enable the assessment of cellular heterogeneity and lead to informed clinical decision-
347 making.

348 First, we aimed to generate scRNAseq-derived gene signatures representative of the
349 cellular heterogeneity present in the TME of advanced HCC¹⁷. Using scRNAseq data
350 from advanced HCC tumours (91,347 cells; scRNAseq Discovery Cohort) and a
351 tailored-bioinformatics pipeline (**Fig. 1**; **Fig. S2A**), we generated gene signatures for
352 35 cell (pheno-)types¹⁷ (**Fig. 2A**), including malignant hepatocytes as well as immune
353 and stromal cell types. Each scRNAseq-derived HCC gene signature consisted of a
354 comparable number of genes, with an average of 36 up-regulated (range 8-110 genes)
355 and 30 down-regulated genes (range 7-125 genes; **Fig. S2B**; **Table S2**). We then
356 evaluated the specificity, robustness, and biological relevance of the resulting HCC
357 gene signatures. To assess the specificity, each signature was categorized as specific
358 or not specific according to its combined expression score per cell (see
359 **Supplementary Methods** for details; **Fig S3** for clarity), and we found 21 of the HCC
360 gene signatures to be specific for their intended cell type (**Fig. 2B**). Gene signatures
361 predicting myeloid subtypes generally performed better than those predicting T-cell
362 phenotypes (**Fig. 2B**; **Fig. S3**), likely due to the higher degree of transcriptomic
363 similarity between distinct T-cell phenotypes. Non-specific signatures were discarded
364 for further downstream analyses. Signature robustness was evaluated using an

365 independent, publicly available scRNAseq cohort of 22 predominantly viral HCCs
 366 (n=45,477 single-cells; scRNAseq Validation Cohort)¹⁸. Firstly, among the 35 cell
 367 types identified in the scRNAseq Discovery Cohort, 31 were also present in the
 368 scRNAseq Validation Cohort (**Fig. S4A-C**). Secondly, the HCC gene signatures
 369 deemed as specific identified the same cell types in both the scRNAseq Discovery and
 370 Validation Cohort, confirming the robustness of our methodology (**Fig. 2C**). The
 371 biological plausibility of each signature, *i.e.* that the genes comprising each signature
 372 were coherent with the corresponding cell phenotype and function, was confirmed
 373 using Enrichr (**Fig. 2D**)²³. Taken together, out of the 35 malignant, immune and stromal
 374 cell types identified in the TME of advanced HCC using scRNAseq, we generated 21
 375 specific, robust and biologically plausible scRNAseq-derived gene signatures that
 376 accurately represent the intra-tumoural cellular heterogeneity of advanced HCC.

377

378 scRNAseq-derived HCC gene signatures and response to atezo+bev in advanced
 379 HCC

380 Next, we used the HCC gene signatures to dissect the intra-tumoural cell type
 381 composition of advanced HCC patients using two bulk RNAseq cohorts, comprising
 382 samples from a total of 422 patients treated with atezo+bev (n=317), atezolizumab
 383 (n=47) or sorafenib (n=58). We aimed to explore the potential of these signatures as
 384 predictors of response to atezo+bev, given that the intra-tumoural presence of specific
 385 cell types has been previously linked to response and/or resistance to therapy¹⁷.

386 Firstly, we collected tumour tissue samples from 96 advanced HCC patients treated
 387 with atezo+bev, of which 71 were subjected to RNAseq (**Inhouse RNAseq Cohort**;
 388 **Fig. S1A**) and 64 remained after quality control filtering. An overview of patient and
 389 tumour characteristics is provided in **Table S3**. Objective response rate (ORR) to

390 atezo+bev was 31% (consistent with results from IMbrave150^{4,5}; **Fig. S1A**), median
391 follow-up was 20 months, and median OS was 14 months. As expected, patients
392 responding to atezo+bev had significantly longer median OS and median PFS
393 compared to non-responders (**Fig. S1B**).

394 A second publicly available RNAseq cohort (**External RNAseq Cohort**) consisting of
395 prospectively collected pre-treatment tumour biopsies of advanced HCC patients
396 treated in the context of the phase Ib (GO30140) and phase III (IMbrave150) trials was
397 used^{4–6,24}. Of the 247 patients treated with atezo+bev and available response data, 81
398 were responders (ORR=33%; **Fig. S1C**). All tissue samples in the External RNAseq
399 Cohort were collected maximum 12 months prior to start of systemic therapy. To
400 maximize the comparability between the two cohorts, we focused our analyses on
401 those samples from the Inhouse RNAseq Cohort that were collected within 12 months
402 of starting atezo+bev treatment (n=39; 11 responders versus 28 non-responders).
403 To explore the potential value of our generated scRNAseq-derived HCC gene
404 signatures in predicting clinical response to atezo+bev, we calculated enrichment
405 scores per sample for each gene signature (**Fig. 3A**; **Fig S5A**). In line with previous
406 findings¹⁷, three cell types, namely two types of CD8+ effector cells (CD8 Temra, CD8
407 Tex) and pro-inflammatory CXCL10+ macrophages (Macro CXCL10), were
408 consistently enriched in atezo+bev responders compared to non-responders in both
409 RNAseq cohorts (**Fig 3B**; **Fig S5B**). Individually, these three signatures identified
410 responders with areas under the curve ranging from 0.63 to 0.79 (**Fig. 3B**; **Fig. S5B**).
411 Notably, the presence of each of the three immune-related signatures was associated
412 with significantly longer PFS upon treatment with atezo+bev, specifically (External
413 RNAseq Cohort, **Fig. S5C**), an association that was not observed with other cell types
414 enriched in responders. The CD8 Temra, CD8 Tex and Macro CXCL10 signatures

415 identified atezo+bev responders with a specificity of 84%-88% (**Fig. 3C**), though their
416 sensitivity was low in both cohorts (**Fig. 3C; Fig. S5D**).
417 Importantly, the three immune-related signatures were strongly correlated (**Fig. S6A-**
418 **B**), suggesting the coexistence of these cell types in the advanced HCC TME. Hence,
419 we classified tumours positive for at least one of the three immune-related signatures
420 as immune-positive tumours (*ImmunePos*), while cases negative for all three immune-
421 related signatures were categorized as immune-negative (*ImmuneNeg*). Compared to
422 *ImmuneNeg* cases, *ImmunePos* tumours had a significantly longer PFS upon
423 treatment with atezo+bev (median PFS 11.1 vs 5.9 months; HR 0.62; 95% CI 0.43-
424 0.90; p=0.011), an association that was not seen in sorafenib-treated patients,
425 supporting the role of an *ImmunePos* status as a predictive biomarker of response to
426 atezo+bev (p of interaction = 0.09; 95% CI 0.234-1.117; **Fig. 3D**).
427

428 Immune versus non-immune mediated response to atezo+bev in advanced HCC
429 In line with the low sensitivity of the *ImmunePos*-defining signatures to identify
430 atezo+bev responders, only 41-55% of responders were classified as *ImmunePos*
431 (33/81 and 6/11 responders in the External and Inhouse RNAseq Cohort,
432 respectively). Importantly, compared to non-responders, *ImmunePos* responders
433 were enriched in the HCC inflamed class (p<0.001)¹⁴ and signatures previously
434 associated with response to anti-PD(L)1 monotherapy in both HCC¹⁰⁻¹³ and other
435 cancer types²⁵⁻²⁹ (**Fig. 4A**). In contrast, *ImmuneNeg* responders were immune cold
436 tumours, displaying a degree of inflammation comparable to that observed in non-
437 responding tumours (**Fig. 4A**), suggesting that distinct mechanisms might underlie
438 response to atezo+bev in *ImmunePos* versus *ImmuneNeg* tumours. To explore this,
439 we first used DGE analysis to compare *ImmunePos* atezo+bev responders to all non-

440 responders regardless of immune status. *ImmunePos* responders were enriched in
441 genes associated with CD8 T-cells (*CD8A*, *CD8B*), cytotoxicity (*PRF1*, *GZMA*, *GZMB*,
442 *GZMH*) and interferon-gamma activity (*GBP1*, *GBP5*), as well as genes involved in T-
443 cell recruitment (*CXCL9/10/11*; **Fig. 4B**). Additional pathway analysis confirmed the
444 enrichment of immune-related related gene sets in *ImmunePos* responders in both the
445 Inhouse and External RNAseq Cohorts (**Fig. 4C; Fig. S6C-D**). Compared to non-
446 responding tumours, *ImmunePos* responders also exhibited a decrease in the
447 expression of genes related to Wnt-β catenin signalling (*GLUL*, *AXIN2*, *DKK4*),
448 previously related to immune cold tumours and ICI monotherapy refractoriness³⁰.
449 Furthermore, we compared atezo+bev-treated patients to a cohort of 28 anti-PD1
450 treated advanced HCC patients (**Anti-PD1 Validation Cohort**) using an unsupervised
451 subclass mapping method (SubMap³¹) and found that anti-PD1 responders were most
452 transcriptomically similar to *ImmunePos* atezo+bev responders (**Fig. 4D**). Taken
453 together, these findings suggest that *ImmunePos* responders may represent tumours
454 more susceptible to the immune activating effect of anti-PD(L)1 treatment.
455 Next, we aimed to identify potential response mechanisms in *ImmuneNeg* responders.
456 Compared to non-responders, *ImmuneNeg* responders displayed an enrichment in
457 signalling pathways related to cell cycle, MYC targets, DNA replication and DNA repair
458 (**Fig. S6E**), suggesting genomic instability. To explore this further, we analysed whole-
459 exome sequencing (WES) data from 67 patients (**External WES Cohort**). *ImmuneNeg*
460 responders tended to be enriched in copy number alterations (CNAs) involving ≥50%
461 of a chromosome arm, as indicated by higher broad CNA scores (BS), compared to
462 both *ImmunePos* responders and non-responders (p=0.16 and p=0.28; **Fig. S7A**).
463 Furthermore, the presence of both high broad CNA loads³² and *TP53* loss-of-
464 heterozygosity (LOH) was significantly higher in *ImmuneNeg* responders (n=7/13,

465 54%) compared to non-responders to atezo+bev (n=10/43, 23%; p=0.046; **Fig. 5A**).
466 This supports the notion that *ImmuneNeg* responders include genetically unstable
467 tumours with *TP53* alterations, previously linked to anti-VEGF response in other
468 cancers³³. Further, it suggests that *ImmuneNeg* responders might be benefitting more
469 from the angiogenesis-related effects of bevacizumab.

470 As bevacizumab targets the VEGF/VEGFR axis, we assessed the expression levels
471 of the VEGF receptors 1-3 and their ligands (**Fig. 5B**; **Fig. S7B**), as well as the VEGF
472 co-receptor neuropilin-1 (*NRP1*; **Fig. 5C**). *ImmuneNeg* responders presented higher
473 *VEGFA* levels compared to *ImmunePos* responders, although no significant
474 differences were observed versus non-responders (**Fig. 5B**). Most notably, and in line
475 with our hypothesis that *ImmuneNeg* atezo+bev responders might be more
476 susceptible to anti-*VEGFA*, we found that *NRP1* expression was significantly lower in
477 this group of patients compared to *ImmunePos* responders and to non-responders
478 (**Fig. 5C**). Low tumour *NRP1* expression is, in fact, one of the most consistently
479 described intra-tumoural biomarkers for bevacizumab response³⁴. Importantly,
480 patients with low *NRP1* tumours had significantly longer PFS and OS upon treatment
481 with atezo+bev (**Fig. 5D-E**), as opposed to sorafenib (p of interaction for OS = 0.039)
482 or atezolizumab monotherapy (**Fig. S7C**). Remarkably, in the scRNAseq Discovery
483 Cohort, we found the highest expression of *NRP1* to be in endothelial cells and
484 pericytes (**Fig. 5F**).

485 Taken together, our findings unveil two distinct mechanisms associated with response
486 to atezo+bev: immune- versus non-immune-mediated response. A first subset of
487 atezo+bev responders are characterized by an immune-rich TME with infiltration of
488 CD8 effector cells and pro-inflammatory macrophages and are identifiable using
489 scRNAseq-derived gene signatures that represent these cell types. A second subset

490 of responders present with genetically unstable tumours lacking the necessary anti-
 491 tumoural immune component, and characterized by a decreased *NRP1* expression.

492

493 Targeting NRP1 in combination with anti-PDL1 + anti-VEGFA remodels the anti-
 494 tumour immune microenvironment in a resistant murine model of HCC

495 To explore whether blocking NRP1 could offer a potential strategy for improving
 496 atezo+bev responses, we generated an orthotopic HCC murine model by implanting
 497 Hep53.4 cells – exhibiting resistance to anti-PDL1 + anti-VEGFA (**Fig. S8**) – into the
 498 livers of C57BL/6J mice (see **Supplementary Methods** for details). Animals were
 499 treated with (i) vehicle; (ii) anti-PDL1 + anti-VEGFA; (iii) an NRP1 inhibitor (EG00229);
 500 or (iv) the triple combination of anti-PDL1 + anti-VEGFA + EG00229 (**Fig. S9A**). Flow
 501 cytometry analysis showed a significant increase in CD8+ T cell subsets in the triple
 502 combination arm compared to vehicle (**Fig. S9B**), an effect not observed with anti-
 503 PDL1 + anti-VEGFA alone. Additionally, tumours from mice treated with anti-PDL1 +
 504 anti-VEGFA + EG00229 presented a higher CD8+/Treg ratio compared to vehicle
 505 ($p=0.015$) and to anti-PDL1 + anti-VEGFA ($p=0.098$) arms (**Fig. S9C**). Overall, these
 506 results indicate that targeting NRP1 in combination with anti-PDL1 + anti-VEGFA
 507 results in a more favourable anti-tumour immune profile, consistent with previous
 508 reports in preclinical melanoma models³⁵.

509

510 Immunosuppressive myeloid cells and stromal populations contribute to primary
 511 resistance to atezo+bev

512 Next, we explored mechanisms associated with primary resistance to atezo+bev.
 513 Using the expression data of all up-regulated genes comprising the 21 specific
 514 scRNAseq-derived HCC signatures, we trained a logistic regression-based machine

515 learning prediction algorithm to discriminate responders from non-responders to
516 atezo+bev (see **Supplementary Methods** for details). The integrated model
517 discriminated atezo+bev responders with an accuracy of 93% (95% CI 0.89-0.96) and
518 82% (95% CI 0.66-0.92) in the training/test and validation cohorts (i.e. the External
519 and Inhouse RNAseq Cohorts), respectively, outperforming previously reported
520 molecular correlates of atezo+bev response (**Fig. S10A**).
521 Out of 686 unique genes used as input, 229 genes were retained as most informative
522 (**Fig. S10B**). Genes associated with known anti-tumoural immune cell types (e.g.
523 CD16+ monocytes) were linked to response to atezo+bev, while genes linked to pro-
524 tumoural, immunosuppressive cell types (e.g. CD14+ monocytes and TREM2+
525 macrophages) were predominantly linked to resistance (**Fig. S11A**). Conversely,
526 genes composing the fibroblasts, endothelial cells or cancer cells signatures did not
527 exhibit a preferential association with response or resistance to atezo+bev, with a
528 similar proportion of genes from these signatures linked to both response and
529 resistance to the combination (**Fig. S10B**). Using pathway analysis, we found that
530 genes within the fibroblast signature associated with primary resistance (n=10) were
531 related to Notch and TGF-β signalling (**Fig. S11B**). Similarly, within the endothelial
532 gene signature, the 19 genes linked to resistance to atezo+bev were related to TGF-
533 β signalling, while the 12 genes linked to response were related to nitric-oxide
534 mediated signalling (**Fig. S11C**), previously associated with bevacizumab efficacy in
535 other tumour types^{36,37}. Of note, genes within the cancer cells signature were linked
536 to metabolic hepatic cell processes regardless of their contribution to response or
537 resistance (**Fig. S11D**). Overall, these data suggest that there are likely distinct
538 subtypes of intra-tumoural endothelial cells or tumour-associated fibroblasts that may
539 play distinct roles in the context of atezo+bev treatment. Additionally, our findings point

540 toward the contribution of stromal-related signalling pathways (Notch and TGF- β) and
541 specific immunosuppressive myeloid populations (CD14+ monocytes and TREM2+
542 macrophages) to resistance to atezo+bev in advanced HCC.

543

544 Finally, we investigated the association between the identified resistance-related
545 features and disease progression (PD) following atezo+bev treatment. Progressors
546 presented a mOS of 7.96 months, contrasting starkly with patients achieving stable
547 disease (SD) (mOS of 18.51 months, p<0.0001; **Fig. S12**). Moreover, in the External
548 RNASeq cohort, 24% of patients with PD upon atezo+bev presented with *ImmunePos*
549 tumours at baseline. Strikingly, *ImmunePos* tumours from progressors were
550 significantly enriched in gene signatures capturing both CD14+ monocytes and
551 TREM2+ macrophages when compared to *ImmunePos* patients who achieved
552 disease control (DC; p=0.034 and p=0.045; **Fig. 6A**). Supporting these observations,
553 multiplex immunohistochemistry revealed a significantly higher ratio of TREM2+
554 macrophages to pro-inflammatory macrophages or to CD8+ T cells in patients with PD
555 versus DC upon atezo+bev (**Fig. 6B-C**).

556 Next, we explored whether *ImmuneNeg* progressors showed an increase in stromal-
557 related signalling pathways such as TGF- β or Notch. Indeed, *ImmuneNeg* patients
558 with PD were characterized by a significant increase in the so-called “late TGF- β
559 signature” – known to be associated with TGF- β oncogenic effects in HCC³⁸ – when
560 compared with *ImmuneNeg* patients with DC (p=0.001; **Fig. 6D, left**). Moreover,
561 *ImmuneNeg* patients with PD exhibited an enrichment in Notch pathway activation²²,
562 compared to *ImmuneNeg* DC patients (p=0.009; **Fig. 6D, right**). In addition, these
563 patients also displayed a higher presence of the progenitor-like Hoshida S2 subclass³⁹
564 (p=0.03; **Fig. 6E**).

565 Consistently, tumours from the syngeneic Hep53.4 model showing anti-PDL1 + anti-
 566 VEGFA resistance (**Fig. S8**) were classified as Notch-active, exhibited high levels of
 567 NRP1, and were enriched in CD14+ monocytes and TREM2+ macrophages, both in
 568 mice treated with vehicle and the combination of anti-PDL1 + anti-VEGFA (**Fig. S13**).
 569 Taken together, our findings identify potential factors contributing to upfront
 570 progressive disease upon atezo+bev treatment in advanced HCC, including the
 571 presence of immunosuppressive immune cell populations such as TREM2+
 572 macrophages and CD14+ monocytes, as well as a stromal contribution stemming from
 573 Notch activation and TGF- β signalling. These insights offer valuable implications for
 574 understanding the intricate mechanisms underlying resistance to atezo+bev in
 575 advanced HCC.

576

577 Defining molecular subsets that determine clinical benefit and primary resistance to
 578 atezo+bev in advanced HCC

579 Finally, we aimed to integrate our findings related to the proposed mechanisms of
 580 response and resistance to atezo+bev to define subgroups of patients that correlate
 581 with therapeutic benefit. To this end, atezo+bev-treated patients from the External
 582 RNAseq Cohort were categorized into three main molecular subsets: “*Immune-*
 583 *competent*”, “*Angiogenesis-driven*” and “*Resistant*” (**Fig. 7A**; see Supplementary
 584 Methods for details) based on i) the presence or absence of immune-promoting versus
 585 immunosuppressive cell types, ii) Notch pathway activation and iii) intra-tumoural
 586 *NRP1* expression levels. Importantly, patients belonging to the “*Immune-competent*”
 587 and “*Angiogenesis-driven*” groups had a significantly longer OS upon atezo+bev
 588 treatment compared to those defined as “*Resistant*” (mOS; not reached versus 11
 589 months; p=0.0001 and p<0.0001 respectively; **Fig. 7B**). These observations were

590 validated when splitting the cohort into patients receiving atezo+bev in the GO30140
591 phase 1b (n=134) versus the IMbrave150 phase III (n=119) trials (**Fig. S14A-B**). Of
592 note, the “*Resistant*” patient group was also associated with a significantly shorter OS
593 when compared to “*Unclassified*” patients (mOS; 11 versus 18.8 months; p=0.005;
594 **Fig. 7B**). Similarly, both the “*Immune-competent*” and “*Angiogenesis-driven*”
595 subgroups presented with significantly longer PFS compared to “*Resistant*” patients
596 (mPFS; not reached versus 2.8 months; p=0.0006 and 7.5 versus 2.8 months;
597 p=0.005, respectively; **Fig. 7C**).

598 Furthermore, patients from the IMbrave150 trial classified as “*Immune-competent*” or
599 “*Angiogenesis-driven*” had significantly longer OS upon atezo+bev treatment
600 compared to sorafenib (p=0.0007; **Fig. 7D**), as opposed to “*Resistant*” or
601 “*Unclassified*” groups. In short, the combined “*Immune-competent*” and
602 “*Angiogenesis-driven*” molecular subgroups demonstrated a significant predictive
603 capacity of clinical benefit to atezo+bev (p of interaction = 0.027; **Fig. 7D**).

604 Altogether, we identified two distinct molecular subsets associated with clinical benefit
605 upon atezo+bev treatment in advanced HCC, each driven by an immune- or
606 angiogenesis-related mechanism. Additionally, we identified the molecular landscape
607 of patients presenting with the poorest survival outcomes after atezo+bev. These
608 findings offer potential applications to molecularly stratify patients based on the
609 efficacy of immunotherapy and antiangiogenic treatments in advanced HCC.

610 **Discussion**

611 Our study is the first to use gene signatures derived from scRNAseq data to accurately
612 identify 21 cell types present in the pre-treatment TME of advanced HCC. We
613 demonstrate their use as invaluable tools to gain insights into the underlying biological
614 mechanisms that drive treatment response and underline their potential clinical
615 application, effectively bridging the gap between scRNAseq and RNAseq data. In
616 doing so, we describe two distinct molecular-based types of response to atezo+bev
617 treatment and define traits characterizing primary resistance.

618 First, approximately 40% of responding tumours were characterized by a pre-existing
619 anti-tumoural immunity defined by the infiltration of CD8+ effector T-cells and pro-
620 inflammatory CXCL10+ macrophages, previously related to atezo+bev response^{6,17}.
621 Additionally, these tumours presented an inflamed microenvironment with molecular
622 features of ICI monotherapy response^{10–13,25–29}, suggesting their susceptibility to the
623 immune-activating effect of atezolizumab.

624 Conversely, the remaining 60% of tumours responding to atezo+bev displayed similar
625 immune infiltration levels to non-responders, but were characterized by genomic
626 instability features including *TP53* alterations, previously associated with anti-VEGF
627 response³³. This subgroup of tumours also showed *NRP1* downregulation, a
628 characteristic previously reported as a biomarker of response to bevacizumab
629 monotherapy³⁴ and associated with longer PFS with bevacizumab treatment in other
630 cancers⁴⁰. Pre-clinical studies have shown that blocking *NRP1* function renders blood
631 vessels more susceptible to anti-VEGF therapy by means of a vascular remodelling
632 process that results in reduced pericyte-vessel associations⁴¹. Consistently, in our
633 data, *NRP1* was mostly expressed in endothelial cells and pericytes. These findings

634 support the notion that clinical benefit in this subgroup of tumours may result from the
635 anti-angiogenic effect of bevacizumab.

636 Whether a subset of responders may benefit from the synergistic effect of both
637 mechanisms is certainly possible, though controversial in a setting where we have
638 phase III data for both ICI monotherapy, anti-VEGFA monotherapy and their
639 combination⁴². In theory, antiangiogenic drugs such as bevacizumab have the
640 capacity to counteract immunosuppressive pathways and restore a functional
641 vasculature to i) improve T cell recruitment into the tumour and ii) increase the
642 bioavailability of anti-PDL1 within the tumour^{6,43,44}. In this case, the resulting
643 therapeutic effect may only be visible within the tumour after treatment, a phenomenon
644 that we cannot capture in the absence of on-treatment tumour samples.

645 Next, we explored the immune cells and pathway-related mechanisms characterizing
646 atezo+bev progressors. We found that the intra-tumoural stromal compartment
647 exhibits unique features associating TGF-β and Notch signalling with resistance to
648 atezo+bev, consistent with previous reports linking these pathways to resistance
649 against anti-PDL1⁴⁵ or anti-VEGFA in other cancers⁴⁶ and HCC⁴⁷.

650 Overall, most atezo+bev progressors (~75%) exhibited low levels of immune infiltration
651 by CD8+ effector T-cells or pro-inflammatory CXCL10+ macrophages. These patients
652 were enriched in Notch signalling and exhibited progenitor-like traits, aligning with
653 previous findings linking high *AFP* and *GPC3* levels to atezo+bev resistance⁶.
654 Surprisingly, ~25% of progressors were infiltrated by CD8+ effector T-cells or pro-
655 inflammatory CXCL10+ macrophages, suggesting the presence of a pre-existing anti-
656 tumoural immunity. Notably, these tumours were also highly infiltrated by two
657 immunosuppressive myeloid cell types, namely TREM2+ macrophages and their
658 precursor, CD14+ monocytes⁴⁸, previously associated with immunotherapy

659 resistance⁴⁹. Moreover, TREM2+ macrophages have been associated with an
660 immunosuppressive role in lung cancer⁵⁰, and found to suppress CD8+ T cell activity
661 and promote anti-PDL1 resistance in HCC patients post-TACE⁵¹. In short, a subset of
662 progressors display a pre-existing immune response that is likely overshadowed by
663 an immunosuppressive myeloid component that contributes to therapeutic inefficacy
664 of atezo+bev in these patients.

665 Finally, by integrating the distinct determinants of response and resistance to
666 atezo+bev, we provide a molecular-based classification comprising three subsets of
667 patients: two subtypes of patients associated with good outcome ("Immune-
668 competent" and "Angiogenesis-driven"), and a "Resistant" subset associated with poor
669 outcome (**Fig. 8**). Importantly, both the "Immune-competent" and "Angiogenesis-
670 driven" subgroups were associated with significantly improved OS upon atezo+bev
671 treatment, with a probability of 80% survival at 20 months (median not reached). In
672 addition, both molecular subgroups were independently associated with improved OS
673 and PFS after atezo+bev when compared to the "Resistant" subgroup, which had
674 significantly worse OS (mOS: 11 months) compared to all other patient groups. In
675 short, we defined novel molecular subsets predictive of clinical outcomes to atezo+bev
676 in advanced HCC using widely accessible transcriptomic analysis, that may help guide
677 clinical decision making in HCC in the future.

678 The main limitation of our study is that to ensure data consistency across cohorts, only
679 samples taken within 12 months of treatment initiation were included, resulting in a
680 limited sample size in the Inhouse RNAseq cohort. Furthermore, our study identifies
681 several factors associated with response or resistance to atezo+bev, but to
682 demonstrate a causal relationship further mechanistic validation experiments are
683 required. Additionally, despite the significant predictive capacity of the proposed

684 molecular subsets to discriminate atezo+bev clinical outcomes, a large proportion of
685 patients remain unclassified. Finally, the limited availability of detailed clinical
686 information from the External RNAseq cohort constrained our ability to conduct a
687 multivariate analysis or assess the potential influence of underlying liver aetiology on
688 the response patterns to atezo+bev observed in this study.

689 In conclusion, we leveraged the resolution of scRNAseq to derive gene signatures and
690 unravel determinants of atezo+bev response and resistance. By integrating our
691 findings, we uncovered both an "*Immune-competent*" and an "*Angiogenesis-driven*"
692 phenotype that derive clinical benefit from atezo+bev, likely due to distinct biological
693 mechanisms. Furthermore, we identified a "*Resistant*" subset associated with poor
694 survival outcomes upon atezo+bev in advanced HCC.

695 **List of abbreviations**

696	ABRS	Atezolizumab + bevacizumab response signature
697	aHCC	advanced HCC
698	Atezo+bev	Atezolizumab + bevacizumab
699	AUC	Area under the curve
700	BS	Broad CNA scores
701	CR	Complete Response
702	CI	Confidence Interval
703	DC	Disease Control
704	DGE	Differential gene expression
705	DEG	Differentially expressed gene
706	FDR	False Discovery Rate
707	FFPE	Formalin Fixed Paraffin-Embedded
708	HCC	Hepatocellular Carcinoma
709	HR	Hazard Ratio
710	ICI	Immune Checkpoint Inhibitors
711	IFNAP	InterFeroN and Antigen-Presentation
712	LOH	Loss of heterozygosity
713	mRECIST	modified Response Evaluation Criteria In Solid Tumours
714	NTP	Nearest Template Prediction
715	NRP1	Neuropilin-1
716	ns	not significant
717	OR	Objective Response
718	OS	Overall Survival
719	PD	Progressive Disease

720	PFS	Progression Free Survival
721	PR	Partial Response
722	RNAseq	bulk RNA sequencing
723	ROC	Receiver operating characteristic curve
724	SD	Stable Disease
725	scRNAseq	single-cell RNA sequencing
726	ssGSEA	single sample Gene Set Enrichment Analysis
727	TACE	Transarterial chemoembolization
728	Teff	T effector cells
729	TME	Tumour microenvironment
730	TGF-β	Transforming growth factor beta
731	Treg	T regulatory cells
732	TKI	Tyrosine Kinase Inhibitors
733	UMAP	Uniform Manifold Approximation and Projection
734	VEGFA	Vascular Endothelial Growth Factor A
735	VEGFR	Vascular Endothelial Growth Factor Receptor

736 **Acknowledgments**

737 We thank Thomas van Brussel, Rogier Schepers and Evy Vanderheyden for all hands-
738 on work related to single-cell experiments. We thank Maria Esteve-García for her
739 support with RNA extractions.

740 This work was supported in part through the computational and data resources and
741 staff expertise provided by Scientific Computing and Data at the Icahn School of
742 Medicine at Mount Sinai and supported by the Clinical and Translational Science
743 Awards (CTSA) grant UL1TR004419 from the National Center for Advancing
744 Translational Sciences. Research reported in this publication was also supported by
745 the Office of Research Infrastructure of the National Institutes of Health under award
746 number S10OD026880 and S10OD030463. The content is solely the responsibility of
747 the authors and does not necessarily represent the official views of the National
748 Institutes of Health.

749 In addition, the study was in part developed in the Centre Esther Koplowitz from
750 IDIBAPS / CERCA Programme / Generalitat de Catalunya.

751 **References**752 **Author names in bold designate shared first authorship**

- 753 1. Sung, Ferlay, Siegel, et al. Global Cancer Statistics 2020: GLOBOCAN
754 Estimates of Incidence and Mortality Worldwide for 36 Cancers in 185 Countries.
755 CA Cancer J Clin 2021;71:209–249.
- 756 2. Llovet, Pinyol, Kelley, et al. Molecular pathogenesis and systemic therapies for
757 hepatocellular carcinoma. Nat Cancer 2022;3:386–401.
- 758 3. Llovet, Ricci, Mazzaferro, et al. Sorafenib in advanced hepatocellular
759 carcinoma. NEJM 2008;359:378–390.
- 760 4. Finn, Qin, Ikeda, et al. Atezolizumab plus Bevacizumab in Unresectable
761 Hepatocellular Carcinoma. NEJM 2020;382:1894–1905.
- 762 5. Cheng, Qin, Ikeda, et al. Updated efficacy and safety data from IMbrave150:
763 Atezolizumab plus bevacizumab vs. sorafenib for unresectable hepatocellular
764 carcinoma. JHep 2022;76:862–873.
- 765 6. Zhu, Abbas, de Galarreta, et al. Molecular correlates of clinical response and
766 resistance to atezolizumab in combination with bevacizumab in advanced
767 hepatocellular carcinoma. Nat Med 2022;28:1599–1611.
- 768 7. Cappuyns, Llovet. Combination Therapies for Advanced Hepatocellular
769 Carcinoma: Biomarkers and Unmet Needs. CCR 2022;28:3405–3407.
- 770 8. Greten, Villanueva, Korangy, et al. Biomarkers for immunotherapy of
771 hepatocellular carcinoma. Nat Rev Clin Oncol 2023;20:780–798.
- 772 9. Llovet, Castet, Heikenwalder, et al. Immunotherapies for hepatocellular
773 carcinoma. Nat Rev Clin Oncol 2022;19:151–172.

- 774 10. Haber, Castet, Torres-Martin, et al. Molecular Markers of Response to Anti-PD1
775 Therapy in Advanced Hepatocellular Carcinoma. *Gastroenterology*
776 2022;S0016-5085:01039–3.
- 777 11. Sangro, Melero, Wadhawan, et al. Association of inflammatory biomarkers with
778 clinical outcomes in nivolumab-treated patients with advanced hepatocellular
779 carcinoma. *JHep* 2020;73:1460–1469.
- 780 12. Neely, Yao, Kudo, et al. Genomic and transcriptomic analyses related to the
781 clinical efficacy of first-line nivolumab in advanced hepatocellular carcinoma
782 from the phase 3 CheckMate 459 trial. AACR Annual Meeting
783 2022;MS.CL11.02.
- 784 13. Spranger, Bao, Gajewski. Melanoma-intrinsic β -catenin signalling prevents anti-
785 tumour immunity. *Nature* 2015;523:231–235.
- 786 14. **Montironi, Castet, Haber**, et al. Inflamed and non-inflamed classes of HCC: a
787 revised immunogenomic classification. *Gut* 2023;72:129–140.
- 788 15. McDermott, Huseni, Atkins, et al. Clinical activity and molecular correlates of
789 response to atezolizumab alone or in combination with bevacizumab versus
790 sunitinib in renal cell carcinoma. *Nat Med* 2018;24:749–757.
- 791 16. Lui, Xun, Ma, et al. Identification of a tumour immune barrier in the HCC
792 microenvironment that determines the efficacy of immunotherapy. *JHep*
793 2023;78:770–782.
- 794 17. Cappuyns, Philips, Vandecaveye, et al. PD-1- CD45RA+ effector-memory CD8
795 T cells and CXCL10+ macrophages are associated with response to
796 atezolizumab plus bevacizumab in advanced hepatocellular carcinoma. *Nat*
797 *Commun* 2023;14:7825.

- 798 18. Ma, Wang, Khatib, et al. Single-cell atlas of tumor cell evolution in response to
799 therapy in hepatocellular carcinoma and intrahepatic cholangiocarcinoma. JHep
800 2021;75:1397–1408.
- 801 19. Llovet, Lencioni. mRECIST for HCC: Performance and novel refinements. JHep
802 2020;72:288–306.
- 803 20. Olbrecht, Busschaert, Qian, et al. High-grade serous tubo-ovarian cancer
804 refined with single-cell RNA sequencing: specific cell subtypes influence survival
805 and determine molecular subtype classification. Genome Med 2021;13:1–30.
- 806 21. **Hao, Hao**, Andersen-Nissen, et al. Integrated analysis of multimodal single-cell
807 data. Cell 2021;184:3573-3587.e29.
- 808 22. Villanueva, Alsinet, Yanger, et al. Notch Signaling Is Activated in Human
809 Hepatocellular Carcinoma and Induces Tumor Formation in Mice.
810 Gastroenterology 2012;143:1660-1669.e7.
- 811 23. Chen, Tan, Kou, et al. Enrichr: interactive and collaborative HTML5 gene list
812 enrichment analysis tool. BMC Bioinformatics 2013;128.
- 813 24. Lee, Ryoo, Hsu, et al. Atezolizumab with or without bevacizumab in
814 unresectable hepatocellular carcinoma (GO30140): an open-label, multicentre,
815 phase 1b study. Lancet Oncol 2020;21:808–820.
- 816 25. Fehrenbacher, Spira, Ballinger, et al. Atezolizumab versus docetaxel for
817 patients with previously treated non-small-cell lung cancer (POPLAR): a
818 multicentre, open-label, phase 2 randomised controlled trial. The Lancet
819 387:1837–46.
- 820 26. Rooney, Shukla, Wu, et al. Molecular and Genetic Properties of Tumors
821 Associated with Local Immune Cytolytic Activity. Cell 2015;160:48–61.

- 822 27. Auslander, Zhang, Lee, et al. Robust prediction of response to immune
823 checkpoint blockade therapy in metastatic melanoma. *Nat Med* 2018;24:1545–
824 1549.
- 825 28. Grasso, Tsoi, Onyshchenko, et al. Conserved Interferon- γ Signaling Drives
826 Clinical Response to Immune Checkpoint Blockade Therapy in Melanoma.
827 *Cancer Cell* 2020;38:500-515.e3.
- 828 29. Ayers, Lunceford, Nebozhyn, et al. IFN- γ -related mRNA profile predicts clinical
829 response to PD-1 blockade. *JCI* 2017;127:2930–2940.
- 830 30. de Galarreta, Bresnahan, Molina-Sánchez, et al. β -catenin activation promotes
831 immune escape and resistance to anti-PD-1 therapy in hepatocellular
832 carcinoma. *Cancer Discov* 2019;9:1124–1141.
- 833 31. Reich, Liefeld, Gould, et al. GenePattern 2.0. *Nat Genet* 2006;38:500–501.
- 834 32. **Bassaganyas, Pinyol, Esteban-Fabró**, et al. Copy-Number Alteration Burden
835 Differentially Impacts Immune Profiles and Molecular Features of Hepatocellular
836 Carcinoma. *CCR* 2020;26:6350–6361.
- 837 33. Wheler, Janku, Naing, et al. TP53 Alterations Correlate with Response to
838 VEGF/VEGFR Inhibitors: Implications for Targeted Therapeutics. *Mol Cancer*
839 *Ther* 2016;15:2475–2485.
- 840 34. Lambrechts, Lenz, De Haas, et al. Markers of response for the antiangiogenic
841 agent bevacizumab. *JCO* 2013;31:1219–1230.
- 842 35. Leclerc, Voilin, Gros, et al. Regulation of antitumour CD8 T-cell immunity and
843 checkpoint blockade immunotherapy by Neuropilin-1. *Nat Commun*
844 2019;10:3345.

- 845 36. Ulivi, Scarpi, Passardi, et al. eNOS polymorphisms as predictors of efficacy of
846 bevacizumab-based chemotherapy in metastatic colorectal cancer: Data from a
847 randomized clinical trial. *J Transl Med* 2015;13:1–10.
- 848 37. Muto, Takagi, Owada, et al. Serum nitric oxide as a predictive biomarker for
849 bevacizumab in non-small cell lung cancer patients. *Anticancer Res*
850 2017;37:3169–3174.
- 851 38. Couloarn, Factor, Thorgeirsson. Transforming growth factor- β gene expression
852 signature in mouse hepatocytes predicts clinical outcome in human cancer.
853 *Hepatology* 2008;47:2059–2067.
- 854 39. Hoshida, Nijman, Kobayashi, et al. Integrative transcriptome analysis reveals
855 common molecular subclasses of human hepatocellular carcinoma. *Cancer Res*
856 2009;69:7385–7392.
- 857 40. Van Cutsem, De Haas, Kang, et al. Bevacizumab in combination with
858 chemotherapy as first-line therapy in advanced gastric cancer: A biomarker
859 evaluation from the AVAGAST randomized phase III trial. *JCO* 2012;30:2119–
860 2127.
- 861 41. Pan, Chanthery, Liang, et al. Blocking Neuropilin-1 Function Has an Additive
862 Effect with Anti-VEGF to Inhibit Tumor Growth. *Cancer Cell* 2007;11:53–67.
- 863 42. Hwangbo, Patterson, Dai, et al. Additivity predicts the efficacy of most approved
864 combination therapies for advanced cancer. *Nat Cancer* 2023;4:1693–1704.
- 865 43. Huinen, Huijbers, van Beijnum, et al. Anti-angiogenic agents — overcoming
866 tumour endothelial cell anergy and improving immunotherapy outcomes. *Nat*
867 *Rev Clin Oncol* 2021;18:527–540.

- 868 44. Fukumura, Kloepper, Amoozgar, et al. Enhancing cancer immunotherapy using
869 antiangiogenics: Opportunities and challenges. *Nat Rev Clin Oncol*
870 2018;15:325–340.
- 871 45. Batlle, Massagué. Transforming Growth Factor- β Signaling in Immunity and
872 Cancer. *Immunity* 2019;50:924–940.
- 873 46. Negri, Crafa, Pedrazzi, et al. Strong Notch activation hinders bevacizumab
874 efficacy in advanced colorectal cancer. *Future Oncol* 2015;11:3167–3174.
- 875 47. Lindblad, Donne, Liebling, et al. NOTCH1 drives sexually dimorphic immune
876 responses in hepatocellular carcinoma. *Cancer Discov* 2024.
- 877 48. Zhou, Wang, Guo, et al. Integrated Analysis Highlights the Immunosuppressive
878 Role of TREM2+ Macrophages in Hepatocellular Carcinoma. *Front Immunol*
879 2022;13:848367.
- 880 49. Tu, Chen, Zheng, et al. S100A9+CD14+ monocytes contribute to anti-PD-1
881 immunotherapy resistance in advanced hepatocellular carcinoma by attenuating
882 T cell-mediated antitumor function. *Journal of Experimental & Clinical Cancer*
883 Research 2024;43:72.
- 884 50. Rodriguez, Chen, Li, et al. Targeting immunosuppressive Ly6C+ classical
885 monocytes reverses anti-PD-1/CTLA-4 immunotherapy resistance. *Front*
886 *Immunol* 2023;14:1161869.
- 887 51. Tan, Fan, Liu, et al. TREM2+ macrophages suppress CD8+ T-cell infiltration
888 after transarterial chemoembolisation in hepatocellular carcinoma. *JHep*
889 2023;79:126–140.

890 **Figure Legends**

891

892 **Fig. 1. Study design**

893

894 **Fig. 2. Identification of specific, robust and biologically plausible single-cell
895 derived HCC gene signatures**896 **2A)** UMAP representation of the 35 cell types identified in the TME.897 **2B)** Overview of HCC gene signatures generated in this study.898 **2C)** Heatmap of the proportion of cells positive for each HCC gene signature,
899 calculated in each cell type, stratified according to signature specificity.900 **2D)** Barplot depicting the top cell types identified for each specific HCC gene signature
901 (n=21) in two single-cell reference datasets, ranked according to adjusted p-value.

902

903 **Fig. 3. Single-cell derived HCC gene signatures and response to atezo+bev**904 **3A)** Heatmap depicting the enrichment of HCC gene signatures in each sample,
905 stratified for response to atezo+bev.906 **3B)** *Top:* Boxplots depicting enrichment scores of CD8 Temra, CD8 Tex and Macro
907 CXCL10, stratified for response to atezo+bev. *Bottom:* Receiver operating
908 characteristic (ROC) curves showing the performance of each signature in predicting
909 response to atezo+bev. Area under the curve (AUC) as indicated.910 **3C)** *Left:* Barplot depicting the presence of CD8 Temra, CD8 Tex and Macro CXCL10
911 in the TME, coloured for response to atezo+bev. *Right:* Sensitivity, specificity, positive
912 and negative predictive value (PPV; NPV), and accuracy of response detection based
913 on the presence of CD8 Temra, CD8 Tex and Macro CXCL10.

914 **3D)** Kaplan-Meier curves depicting progression free survival (PFS) of *ImmunePos*
 915 versus *ImmuneNeg* tumours in patients treated with atezo+bev (n=253, *left*) versus
 916 sorafenib (n=58, *right*).

917 *Statistics:* 3A-B: student *T-test*, Welch's *T-test* or Wilcoxon rank sum test, as
 918 appropriate. C: Fisher's exact test. D: HR, 95% CI and p-values calculated using a
 919 univariate cox regression analysis.

920

921 **Fig. 4. Immune-mediated response to atezo+bev in advanced HCC**

922 **4A)** Heatmap representation of HCC inflamed (sub)classes and gene signatures
 923 previously associated with response to anti-PD(L)1 monotherapy in *ImmunePos* and
 924 *ImmuneNeg* responders versus non-responders to atezo+bev.

925 **4B)** Volcano plot depicting differentially expressed genes between *ImmunePos*
 926 responders (n=33) and non-responders (n=166) to atezo+bev.

927 **4C)** Pathways enriched based on differentially upregulated genes in *ImmunePos*
 928 responders (n=733 genes) versus non-responders to atezo+bev (n=166 genes),
 929 identified in Fig. 4B.

930 **4D)** SubMap analysis evaluating transcriptomic similarity between response groups in
 931 atezo+bev- versus anti-PD1- treated patients. FDR-corrected p-values are shown.

932 *Statistics 4A: student T-test, Welch's T-test, Wilcoxon rank sum test or Fisher's exact*
 933 *test, as appropriate.*

934

935 **Fig. 5. Angiogenesis-related response to atezo+bev in advanced HCC**

936 **5A)** Barplot representing the number of patients presenting both high broad CNA loads
 937 and *TP53* loss-of-heterogeneity across response subgroups.

938 **5B)** Boxplots depicting *VEGFA* expression levels across atezo+bev response groups.

939 **5C)** Boxplots depicting *NRP1* expression levels across atezo+bev response groups.

940 **5D)** Kaplan-Meier curves depicting progression free survival (PFS) of atezo+bev
941 treated patients (n=253) according to low *NRP1* expression status.

942 **5E)** Kaplan-Meier curves depicting overall survival (OS) of atezo+bev treated patients
943 (n=253) according to low *NRP1* expression status.

944 **5F)** *Top:* UMAP representation of *NRP1* expression in the TME. *Bottom:* Heatmap of
945 *NRP1* expression in each cell type identified in the TME.
946 *Statistics:* 5A: Fisher's exact test; 5B-C: Kruskal-Wallis test followed by Dunn-test
947 adjusted by Benjamini-Hochberg. E-F: HR, 95% CI and p-values calculated using a
948 univariate cox regression analysis.

949

950 **Fig. 6. Determinants of primary resistance to atezo+bev in advanced HCC**

951 **6A)** Boxplot depicting the enrichment CD14+ monocytes and TREM2+ macrophages
952 in patients with *ImmunePos* tumours with progressive disease (PD) versus disease
953 control (DC) after atezo+bev.

954 **6B-C)** Boxplot depicting the ratio of TREM2+ macrophages to pro-inflammatory
955 macrophages (B) and to CD8+ T cells (C), with representative images.

956 **6D)** Boxplot depicting the enrichment of the Late TGF- β signature (*left*) and barplot
957 showing the frequency Notch pathway activation (*right*) in patients with *ImmuneNeg*
958 tumours with PD versus DC after atezo+bev.

959 **6E)** Barplot displaying the frequency of S1, S2 or S3-classified tumours amongst
960 patients who showed PD versus DC after atezo+bev.
961 *Statistics:* 6A-E: student T-test, Welch's T-test or Wilcoxon rank sum test or Fisher's
962 exact test, as appropriate.

963

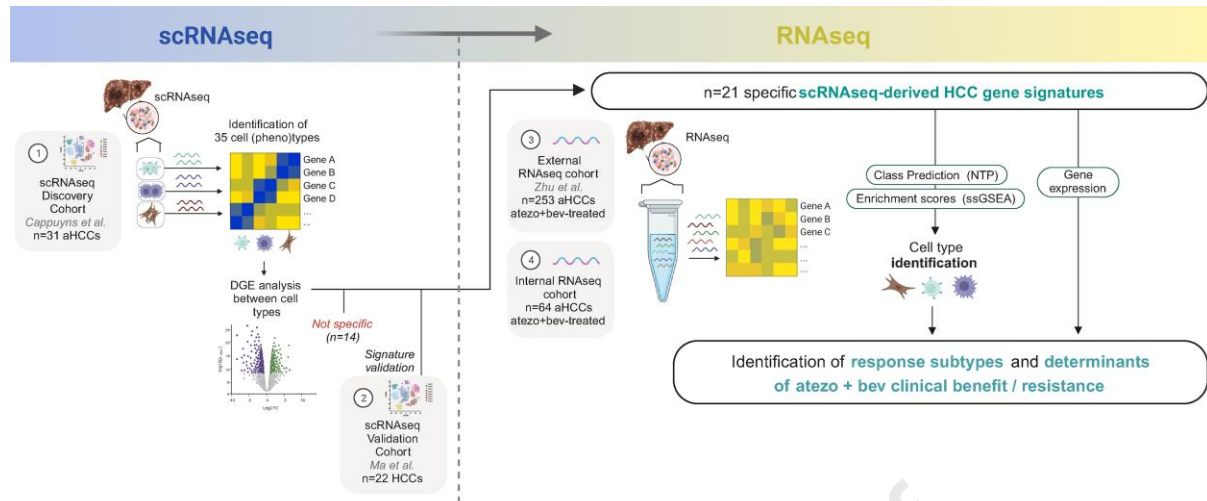
964 **Fig. 7. Molecular subsets determine clinical outcomes to atezo+bev in advanced**
965 **HCC**

966 **7A)** Flowchart summarising the classification criteria into the distinct molecular
967 subsets, defined by: ¹Presence of CD8 Temra, CD8 Tex, or Macro CXCL10; ²Absence
968 of CD8 Temra, CD8 Tex or Macro CXCL10; ³Absence of CD14+ monocytes or
969 TREM2+ macrophages; ⁴Presence of CD14+ monocytes or TREM2+ macrophages;
970 Absence⁵ or presence⁶ of Notch; Decreased *NRP1* expression⁷ or not⁸.

971 **7B-C)** Kaplan-Meier curves depicting overall survival (OS) and progression-free
972 survival (PFS) of atezo+bev treated patients (n=253) according to molecular subset.

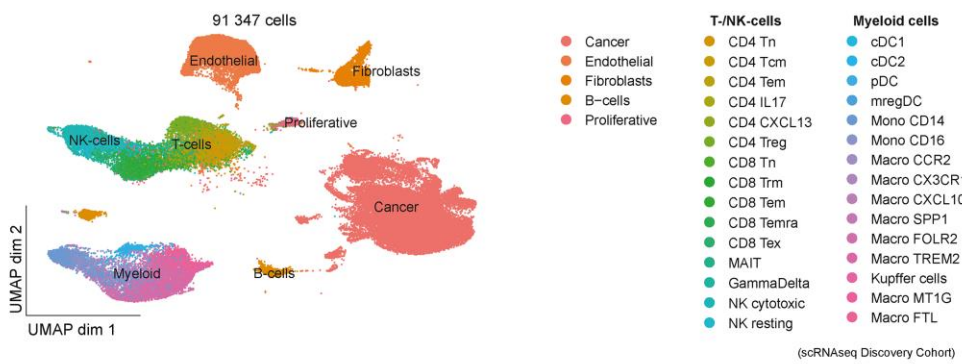
973 **7D)** Kaplan-Meier curves depicting OS in the IMbrave150 study (n=177) stratified
974 according to "*Immune-competent*" and "*Angiogenesis-driven*" (*left*) or "*Unclassified*"
975 and "*Resistant*" (*right*) classification.

976 *Statistics: 7B-C: log-rank test with BH-adjustment. 7D: log-rank test. P of interaction*
977 *calculated using a Cox proportional hazards model.*

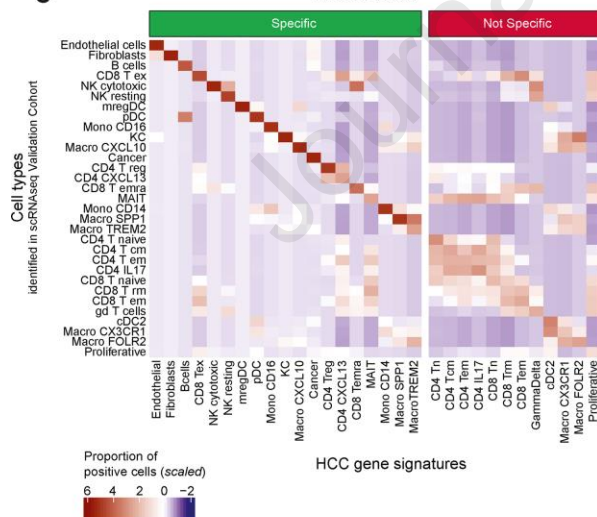
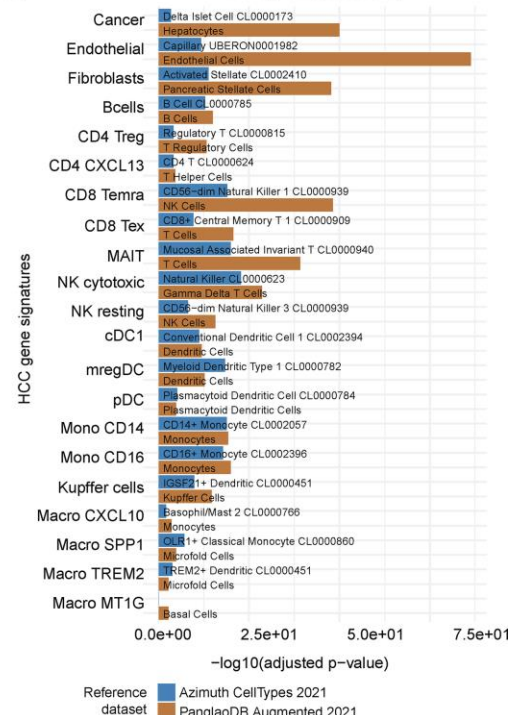


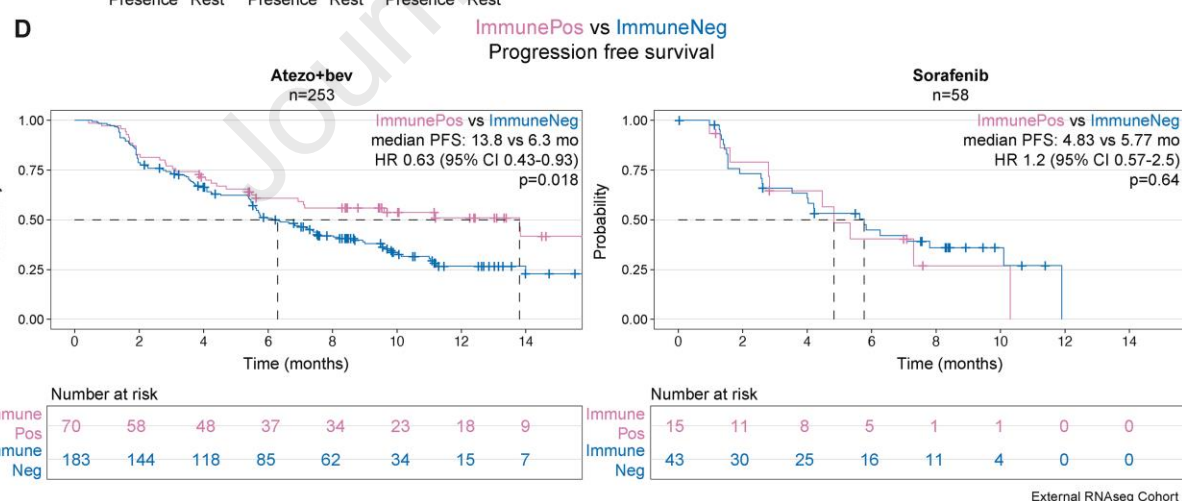
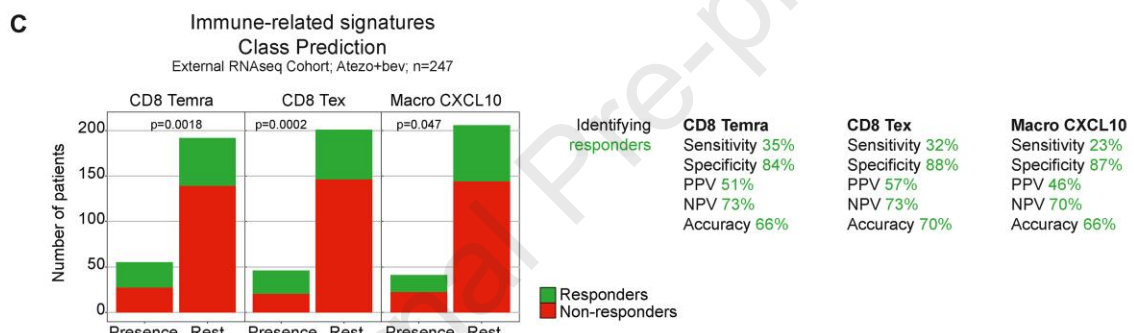
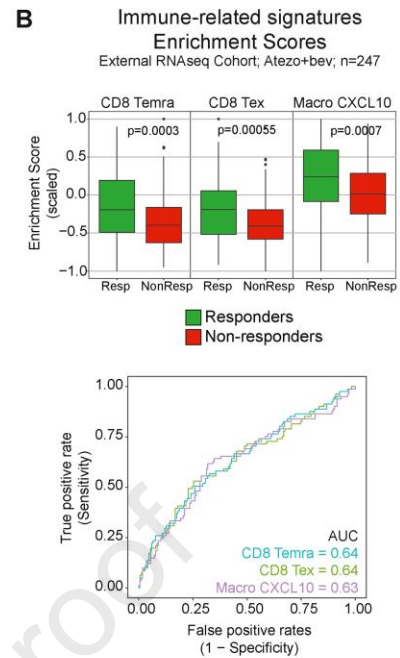
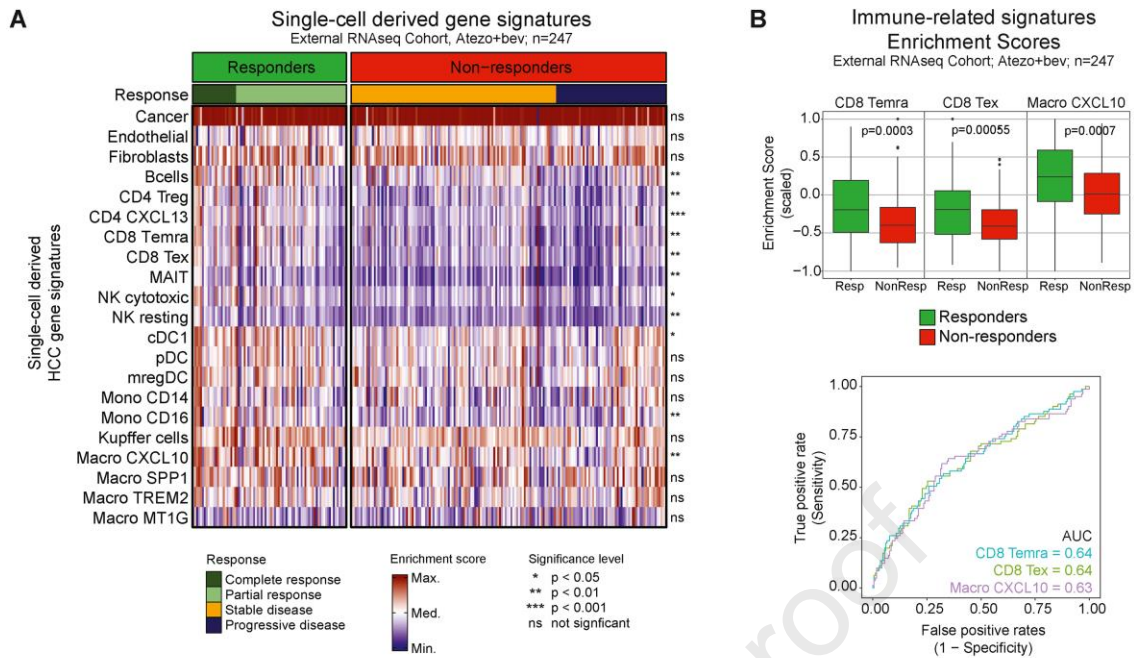
A The tumour-microenvironment of advanced HCC

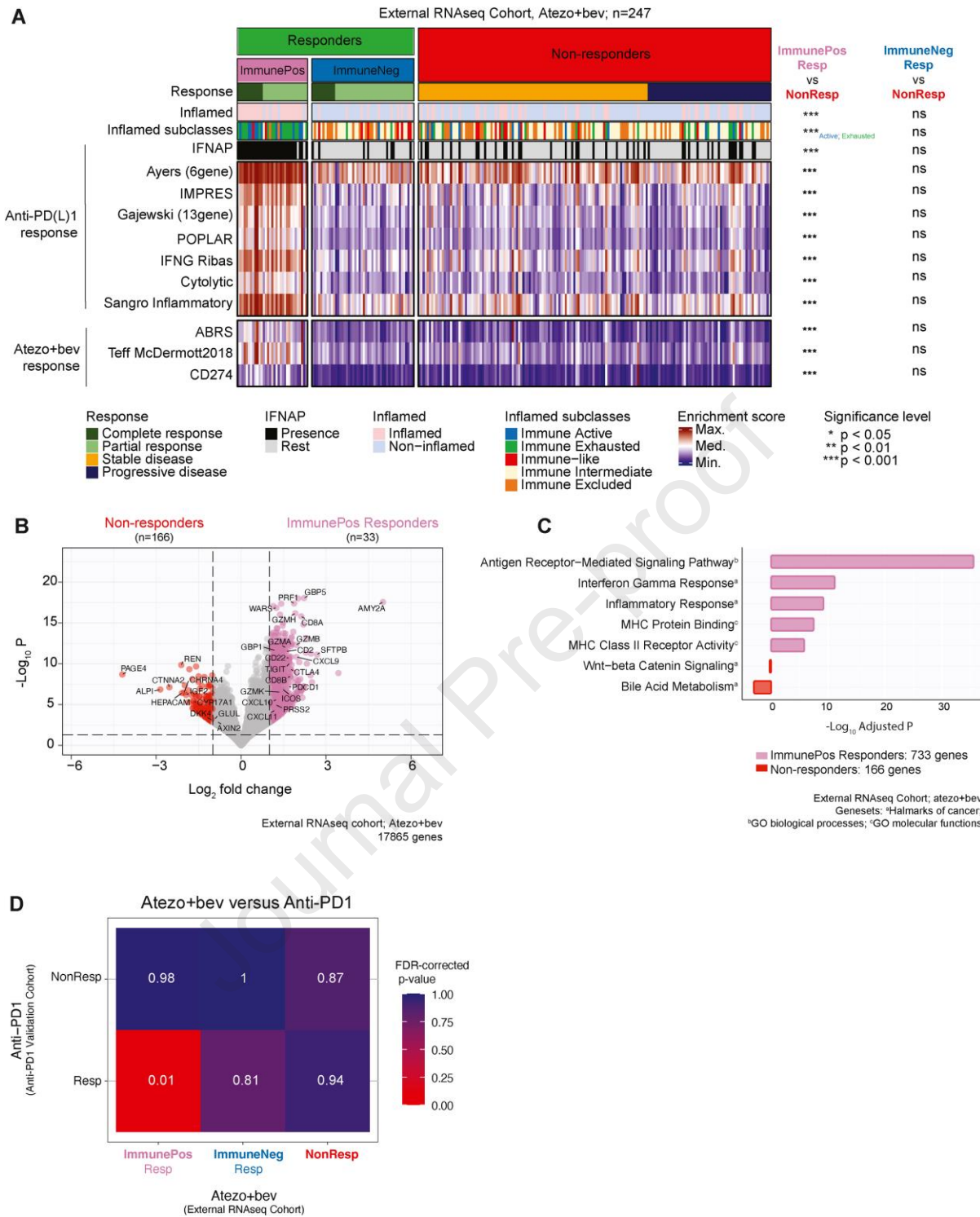
35 distinct cell (pheno-)types

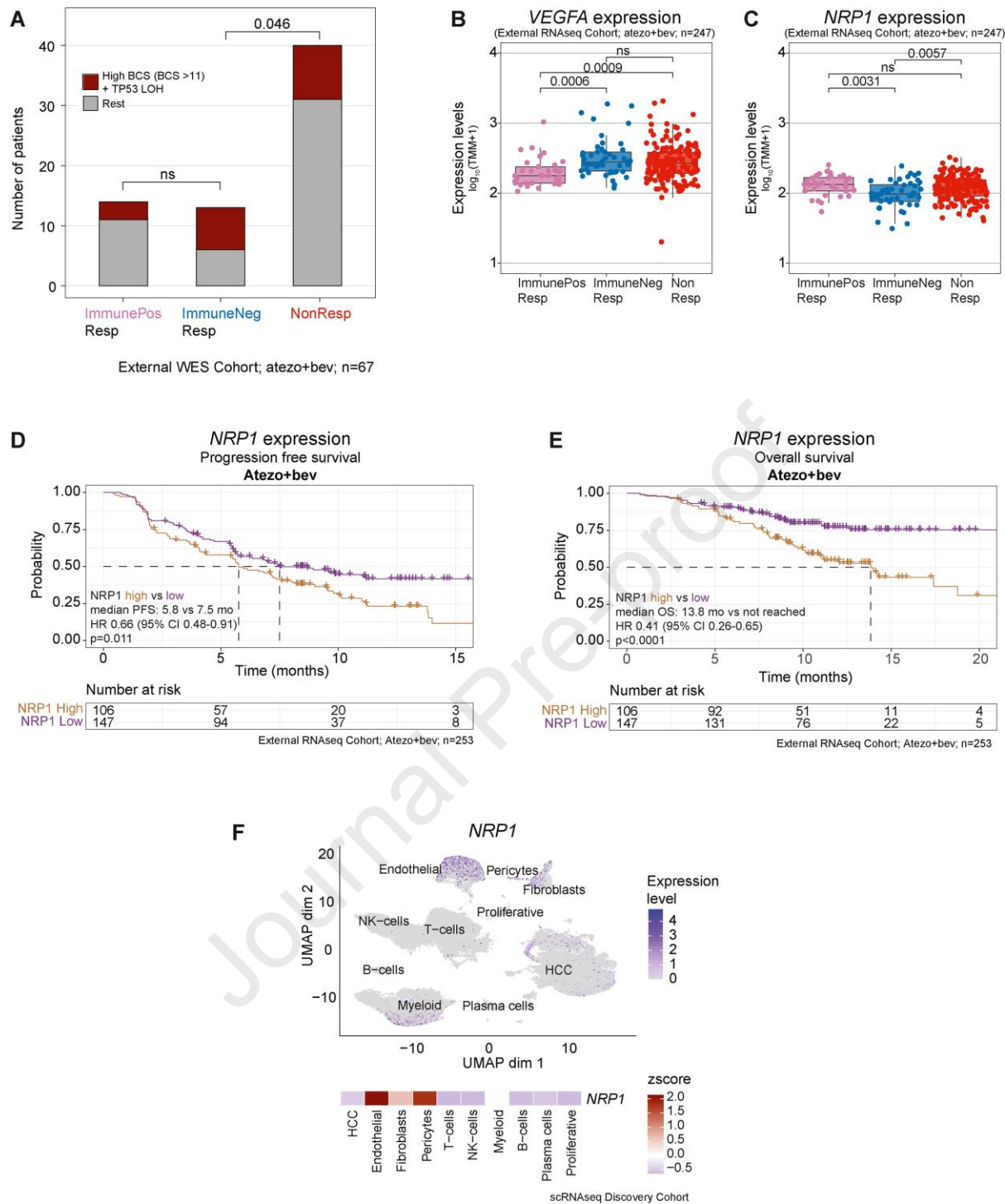
**B Specificity**

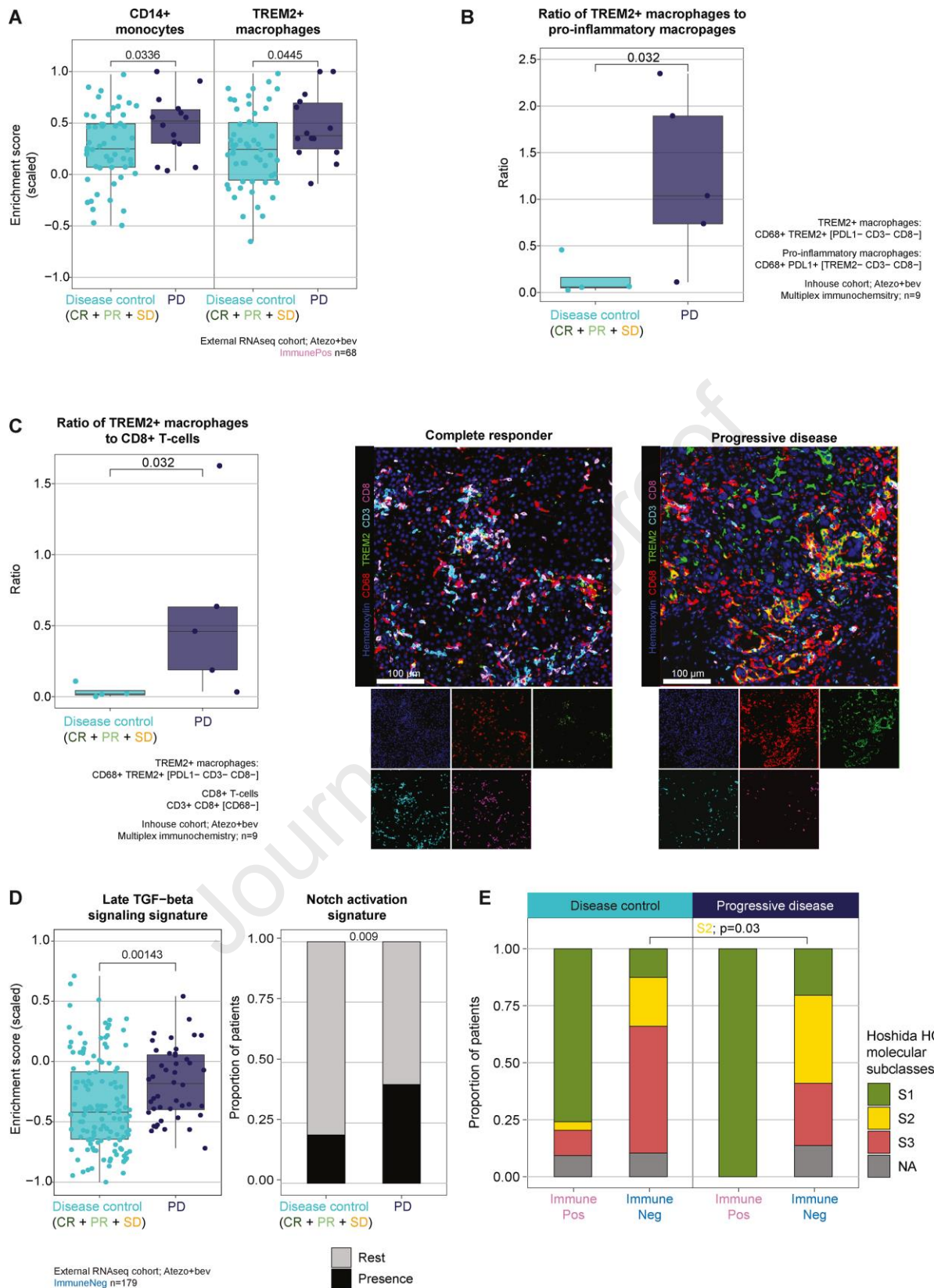
Single-cell derived gene signatures	
Specific (n=21)	Not Specific (n=14)
Endothelial	Cancer
Fibroblasts	CD4 Tn
B-cells	CD4 Treg
CD8 Tex	CD4 Tem
NK cytotoxic	CD4 IL17
NK resting	MAIT
cDC1	CD8 Trm
pDC	CD8 Tem
mregDC	GammaDelta
Mono CD16	Proliferative
Kupffer cells	cDC2
Macro CX3CR10	CD8 Tex
Macro MT1G	Macro CCR2
	Macro CX3CR1
	Macro FOLR2
	Macro FTL

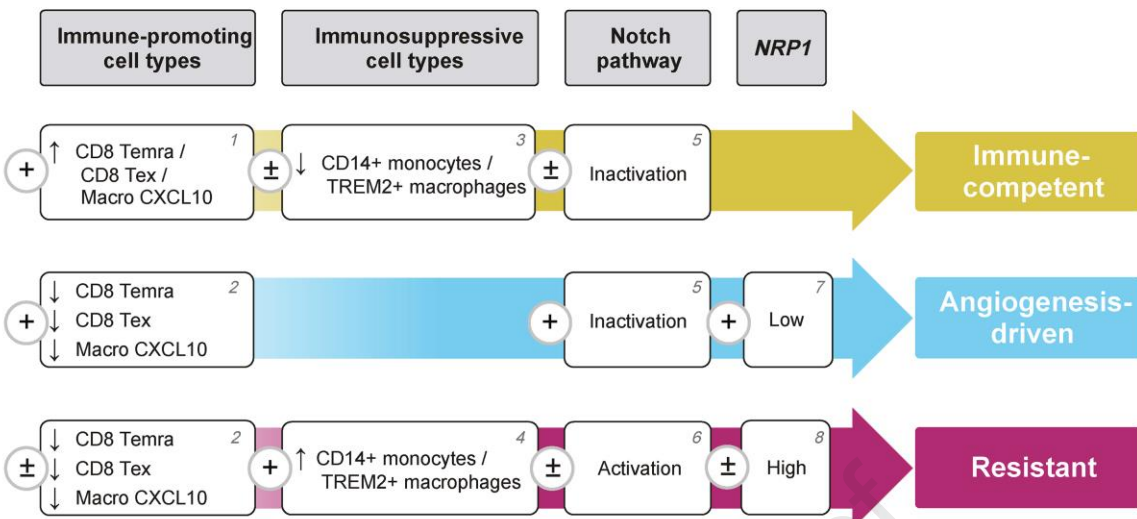
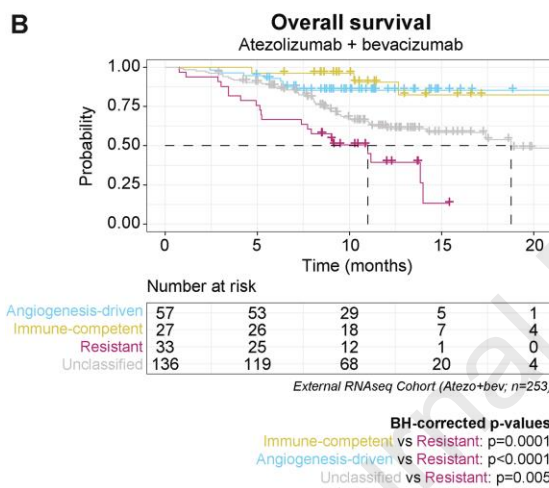
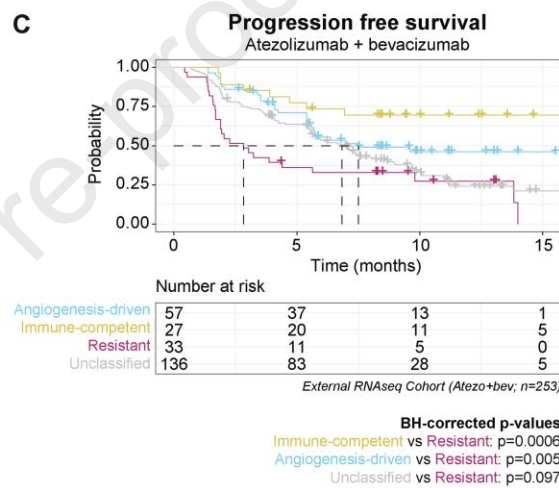
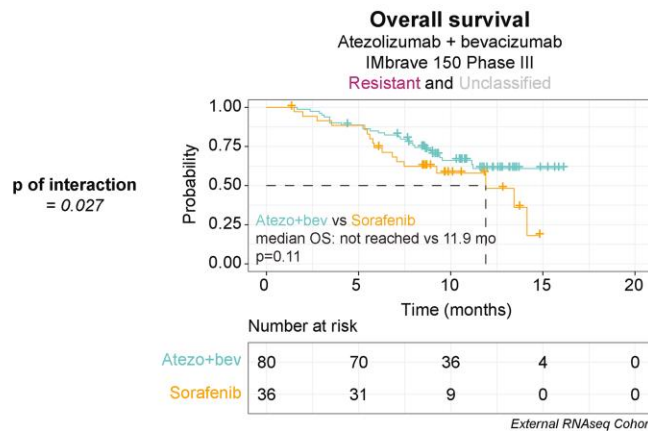
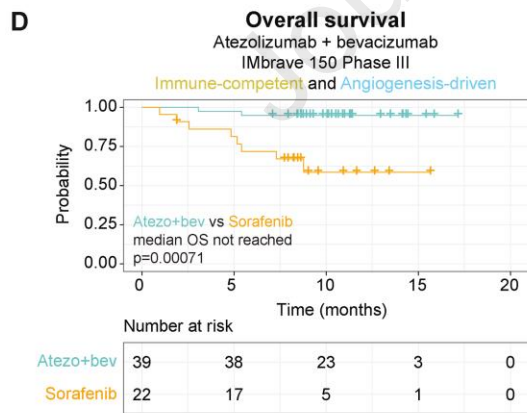
C Robustness**D Biological plausibility**









A**B****C****D**

Highlights

- Single-cell-derived gene signatures were identified for 21 cell types in the advanced HCC TME
- Response to atezo+bev is driven by two distinct mechanisms: Immune- versus angiogenesis-driven
- Immunosuppressive myeloid cells and Notch activation contribute to therapy resistance
- Molecular stratification determines clinical outcome with atezo+bev in advanced HCC